J. Fluid Mech. (1978), *vol.* 86, *part* 1, *pp.* 67–108
Printed in Great Britain

The fine-scale structure of the turbulent velocity field

By F. H. CHAMPAGNE

Department of Applied Mechanics and Engineering Sciences,
University of California, La Jolla

(Received 9 June 1977)

The existence of universal similarity of the fine-scale structure of turbulent velocity fields and the validity of the original Kolmogorov local similarity theory and the later reformulations were investigated. Recent studies of the fine-scale velocity field for many different flows, e.g. grid flows, wakes, jets and the atmospheric boundary layer, are shown to provide considerable evidence for the existence of Kolmogorov normalized spectral shapes which are universal in the sense that they describe the high wavenumber spectral behaviour of all turbulent flow fields with a similar value of the turbulence Reynolds number R_λ. The normalized spectral shapes vary with R_λ in a manner consistent with the later reformulations. The Reynolds number dependence of the normalized spectra is demonstrated for the R_λ range from about 40 to 13000. Expressions for the Kolmogorov normalized spectral functions are presented for three values of R_λ. Also revealed in this study is the importance of considering effects on spectra caused by deviations from Taylor's approximation in high intensity turbulent flows. Lumley's (1965) model is used to correct the high frequency portion of the measured one-dimensional spectra for these effects. An analytical solution to Lumley's expression is presented and applied to the data.

1. Introduction

For many years a number of investigators have attempted to measure the high wavenumber region of the one-dimensional spectra of the velocity-component fluctuations in various turbulent shear flows. Knowledge of the fine-scale structure is important as a basis for developing new turbulence theories, as well as testing existing ones, and for other applications such as the inertial-dissipation and direct-dissipation techniques for estimating the turbulent flux of momentum in the atmospheric surface layer (Champagne *et al.* 1977).

The statistical properties of the fine-scale structure of the turbulent velocity field are a particular area of turbulence research where significant data are still lacking. The validity and/or limitations of the universal similarity theory of Kolmogorov (1941) and the refinements by Kolmogorov (1962), Oboukhov (1962) and Yaglom (1966) are still under investigation. The spatial randomness of dissipation, not considered in the early universal similarity theory, was accounted for in the subsequent refinements or new similarity framework. Kolmogorov's similarity theories are one of the simplest, yet most powerful, parts of turbulence theory and therefore further accurate and relevant data regarding their validity should be obtained.

As the similarity theories are formulated for high Reynolds number velocity fields, experimental investigation of their validity should be carried out in the highest

Reynolds number flows available. An example of such a flow is the atmospheric boundary layer, which provides turbulence Reynolds numbers an order of magnitude larger than those obtained in the laboratory. Further, as Wyngaard & Tennekes (1970) have shown that within the new similarity framework the fine-scale structure is Reynolds number dependent, the investigation should include data covering a wide range of Reynolds numbers to determine the possible dependence. The purpose of the present study is to provide some new data on both the atmospheric turbulent boundary layer and various laboratory flows, and to examine these data together with already existing data for evidence of universal behaviour and local isotropy in the fine-scale structure of the turbulent velocity field.

2. Theoretical and experimental background

The local similarity or universal equilibrium theory predicts the existence of an equilibrium range of (high) wavenumbers which is independent of the energy-containing range of wavenumbers or large-scale features of the flow when the Reynolds number is large enough. Kolmogorov's (1941) original theory consists of two hypotheses concerning the fine-scale structure or equilibrium range of wavenumbers in turbulence of sufficiently large Reynolds number. The first hypothesis states that the motion associated with the equilibrium range of wavenumbers is isotropic and uniquely determined statistically by ϵ, the viscous dissipation of turbulent energy, and ν, the kinematic viscosity. A transformation of space and time to co-ordinates normalized by the Kolmogorov length $\eta = (\nu^3/\epsilon)^{\frac{1}{4}}$ and time $(\nu/\epsilon)^{\frac{1}{2}}$ should reduce the probability density functions describing the small-scale turbulence to universally similar forms, as well as all statistical parameters derived from the probability laws. In particular, the one-dimensional spectrum function takes the form

$$F_1(k_1) = (\epsilon\nu^5)^{\frac{1}{4}}\Phi_1(\eta k_1), \tag{1}$$

where

$$\overline{u_1^2} = \int_0^\infty F_1(k_1)\,dk_1. \tag{2}$$

u_1 is the velocity fluctuation component in the mean flow direction x_1. For high enough Reynolds number, the Kolmogorov normalized spectrum function $\Phi_1(\eta k_1)$ should be a universal function valid for all turbulent velocity fields in their equilibrium range of wavenumbers. The Reynolds number used to characterize the turbulence is R_λ, defined by

$$R_\lambda = (\overline{u_1^2})^{\frac{1}{2}}\lambda_g/\nu, \tag{3}$$

where λ_g is the transverse Taylor microscale (Corrsin 1959).

The second hypothesis postulates the existence of a wavenumber subrange within the equilibrium wavenumber region where the effects of viscosity are negligible. Within the subrange, called the inertial subrange, transfer of energy by inertial forces is the dominant process. Dimensional analysis leads to the renowned $-\frac{5}{3}$ law

$$F_1(k_1) = \alpha_1\epsilon^{\frac{2}{3}}k_1^{-\frac{5}{3}}, \tag{4}$$

where α_1 is a universal constant.

Kolmogorov (1962) refined his original theory to take into account the spatial randomness or variability of the dissipation rate. Kolmogorov's modified or third

hypothesis states that the locally averaged dissipation rate is a lognormal random variable with variance

$$\sigma^2 = A + \mu \ln (L/r), \quad L \ll r \ll \eta^{-1}, \tag{5}$$

where μ is a universal constant, L is the integral scale of the flow, A is a constant depending on flow geometry, and r is the characteristic length of the averaging volume. Yaglom (1966), using assumptions regarding the characteristic length scales of the averaging volumes, deduced a modified inertial-subrange form to be

$$F_1(k_1) = C_2 \epsilon^{\frac{2}{3}} k_1^{-\frac{5}{3}} (L k_1)^{-\frac{1}{6}\mu}, \tag{6}$$

where C_2 is a constant.

An essential part of these theories is the postulate of local isotropy; that is, at sufficiently large Reynolds number, the small-scale turbulent structure is isotropic even when the large-scale structure is not. Many kinematic conditions are imposed on the turbulent velocity field by the assumption of local isotropy. Some of these conditions are that the odd moments of variables such as $\partial u_i/\partial x_j$, $i \neq j$, are identically zero and that the streamwise derivatives of the velocity components are related by

$$\overline{\left(\frac{\partial u_1}{\partial x_1}\right)^2} = \frac{1}{2}\overline{\left(\frac{\partial u_2}{\partial x_1}\right)^2} = \frac{1}{2}\overline{\left(\frac{\partial u_3}{\partial x_1}\right)^2}. \tag{7}$$

As a result the average rate of energy dissipation can be obtained from

$$\epsilon = 15\nu\overline{(\partial u_1/\partial x_1)^2}. \tag{8}$$

Further, according to the isotropic assumption the spectra of the cross-stream velocity components should satisfy the relations

$$F_2(k_1) = F_3(k_1) = \tfrac{1}{2}[F_1(k_1) - k_1\, \partial F_1(k_1)/\partial k_1]. \tag{9}$$

The criteria used most widely to test for the existence of local isotropy result from combining (9) and (4), which gives

$$F_2(k_1) = F_3(k_1) = \tfrac{4}{3}F_1(k_1) \tag{10}$$

for the inertial wavenumber region.

Precise experimental support for local similarity of the velocity fields is not available, even though in the early 1960s it was shown that the available turbulence measurements were consistent with Kolmogorov's original theory within the limited accuracy available (Grant, Stewart & Moilliet 1962; C. H. Gibson & Schwarz 1963; M. M. Gibson 1963). The $-\frac{5}{3}$ inertial-subrange form (4) was observed in fully developed turbulent pipe flow by Laufer (1954), in the atmospheric boundary layer by Taylor (1955), in a tidal channel by Grant *et al.* (1962), in an axisymmetric jet by M. M. Gibson (1963), in the atmospheric boundary layer over the open ocean by Pond, Stewart & Burling (1963) and Pond, Smith, Hamblin & Burling (1966), in a fully developed turbulent channel flow by Comte-Bellot (1965), in a laboratory boundary layer by Bradshaw (1966), in the turbulent wake of a circular cylinder by Uberoi & Freymuth (1969), in a nearly homogeneous uniform shear flow by Champagne, Harris & Corrsin (1970), and in the atmospheric boundary layer by Gibson, Stegen & Williams (1970), Kaimal *et al.* (1972), Boston & Burling (1972), Busch (1973), Williams & Paulson (1976) and Champagne *et al.* (1977). In many of the above cases, however, the $-\frac{5}{3}$-law form extended far into the lower wavenumber region where the flows were

clearly anisotropic from consideration of various necessary conditions for the existence of local isotropy (Corrsin 1957; Lumley 1964), and where (9) was not satisfied. This has led to the conclusion that the apparent existence of a Kolmogorov $-\frac{5}{3}$ law, even with a proper 'universal' constant magnitude, is a relatively insensitive indicator of local isotropy (Bradshaw 1967; Champagne *et al.* 1970; Busch 1973).

The spectral relations (10) were apparently verified for a jet flow by Gibson (1963), although Comte-Bellot (1965) found F_3/F_1 to be about 0·9 in fully developed channel flow. Elderkin (1966) and Weiler & Burling (1967) indicated that their spectral data for the atmospheric boundary layer were not consistent with (10). Champagne *et al.* (1970) found reasonable agreement with the isotropic spectral relations (9) in their low Reynolds number flow. More recently, Kaimal *et al.* (1972) found agreement with (10) in the atmospheric boundary layer under unstable conditions and an approach to (10) under stable conditions, but their $\overline{u_3^2}$ spectral measurements were confined to the lower wavenumber end of the apparent inertial subrange by use of a sonic anemometer with a spatial resolution of about 20 cm. Several other atmospheric results pertaining to the validity of (10) are discussed in the paper of Kaimal *et al.* as well as by Busch (1973). Direct experimental verification of local isotropy in laboratory or atmospheric flows through measurements of the various statistics presented above is a difficult task. Velocity sensors with spatial resolution to about the Kolmogorov length scale η, typically of the order of 1 mm in atmospheric boundary layers and 0·1–0·2 mm or smaller in most laboratory flows, are necessary to measure velocity derivatives adequately. Some of the other problems associated with measuring fine-scale properties of turbulent velocity fields are discussed by Tennekes & Wyngaard (1972). As a result, few of the velocity-derivative statistics have been satisfactorily measured, especially in high Reynolds number flow fields.

Experimental investigations of the validity of the refined similarity theory have been performed by many workers, including Gibson *et al.* (1970), Stewart, Wilson & Burling (1970), Wyngaard & Tennekes (1970), Sheih, Tennekes & Lumley (1971), Wyngaard & Pao (1972) and Kuo & Corssin (1972), whose results would tend to favour the refined formulation. The universal constant μ has been determined to be roughly 0·5 (Gibson & Masiello 1972), so the wavenumber exponent in the modified inertial-subrange form (6) changes from $-\frac{5}{3}$ by $-\frac{1}{18}$, which is certainly a difficult if not impossible change to detect in most realizable high Reynolds number flows.

One of the most significant consequences of this refinement is that it implies that the fine-scale structure is Reynolds number dependent. Kuo (1970) measured the flatness factor or kurtosis of both the first and the second derivative of u_1 in laboratory flows for a range of the turbulence Reynolds number R_λ from 12 to 830. The kurtosis of both derivatives monotonically increased with R_λ and no sign of an approach to asymptotic values was observed. Wyngaard & Tennekes (1970), assuming that the logarithm of the locally averaged dissipation rate was normally distributed with a variance increasing with R_λ, predicted the skewness S and kurtosis K of $\partial u_1/\partial x_1$ to increase in a power-law manner with increasing R_λ, and also that $-S \propto K^{\frac{3}{2}}$. Their results successfully predicted the trends of the existing laboratory data, including those of Kuo (1970), and the high Reynolds number data for the atmospheric surface layer with R_λ values up to 10^4. Further, Wyngaard & Tennekes (1970) noted that their results imply that the Kolmogorov normalized spectrum is Reynolds number dependent, in direct conflict with the original universal-equilibrium theory. This can be demonstrated by considering the

equation for the mean-square fluctuating vorticity, which for steady flows of sufficiently high Reynolds number can be approximated by (see Tennekes & Lumley 1972, p. 91)

$$\overline{\omega_i \omega_j \frac{\partial u_i}{\partial x_j}} = \nu \overline{\frac{\partial \omega_i}{\partial x_j} \frac{\partial \omega_i}{\partial x_j}}, \tag{11}$$

where $\omega_i = \epsilon_{ijk} \partial u_k / \partial x_j$. For locally isotropic turbulence (11) can be written in the form (Wyngaard & Tennekes 1970; Panchev 1971, p. 183)

$$S\left(\frac{\partial u_1}{\partial x_1}\right) = -116 \int_0^\infty (\eta k_1)^4 \Phi_1(\eta k_1)\, d(\eta k_1). \tag{12}$$

Local isotropy places an additional constraint on the normalized spectrum function given by

$$\tfrac{1}{15} = \int_0^\infty (\eta k_1)^2 \Phi_1(\eta k_1)\, d(\eta k_1), \tag{13}$$

which can be obtained from (8). As the available data indicate that $-S$ increases with R_λ, Wyngaard & Tennekes (1970) and Wyngaard & Pao (1972) concluded from (12) and (13) that the shape of the normalized spectrum function varies with Reynolds number, especially in the dissipative wavenumber region. They pointed out that further definitive experiments providing high-quality data on fine-scale structure were necessary to determine the Reynolds number dependence of the normalized spectrum function.

3. Data interpretation

The measurements to be considered represent the temporal variation of a signal from a hot-wire anemometer (or X-array) located at a fixed point in a flow field. As the theoretical relations presented above are concerned with the spatial or wavenumber behaviour of the fine-scale velocity field, the spatial variation of the velocity signal must be deduced from the time-varying signal. This presents two problems: first, how to relate the hot-wire anemometer signal to the velocity; second, how to interpret the time variation of the signal in terms of spatial variation. Another consideration is that the hot-wire sensing length is typically larger than Kolmogorov's length scale η, so that distortion of the measurements of the smallest scales in the flow can occur. These problems are important in the study of the fine-scale structure of the velocity field and will be considered in this section.

Taylor's (1938) approximation is commonly written in the form

$$\partial/\partial t = -\overline{U}_1 \partial/\partial x_1, \tag{14}$$

where $\overline{U}_1$ is the mean speed in the x_1 direction and t is time, or in the wavenumber form

$$k_1 = 2\pi f/\overline{U}_1, \tag{15}$$

where k_1 is the x_1 component of the wavenumber vector and f is the frequency. Equation (14) involves some tacit assumptions as written so a simple derivation of Taylor's 'frozen-flow' approximation will be given. Let $(\mathbf{x}, t)$ be the fixed laboratory reference

system and let $(\mathbf{x}', \tau)$ be a co-ordinate system convected at a *steady* convection velocity $\mathbf{V}$. Therefore, in the moving frame

$$\mathbf{x}' = \mathbf{x} - \mathbf{V}t, \tag{16}$$

$$\mathbf{U}'(\mathbf{x}', \tau) = \mathbf{U}(\mathbf{x}, t) - \mathbf{V}, \tag{17}$$

where $\mathbf{U}(\mathbf{x}, t)$ is the fluid velocity in the fixed reference frame. Let $\tau = t$ so that the frames will coincide at $t = \tau = 0$.

Decomposition of the instantaneous velocity vectors in terms of their mean and fluctuating components gives

$$\overline{\mathbf{U}}'(\mathbf{x}', \tau) = \overline{\mathbf{U}}(\mathbf{x}, t) - \mathbf{V}, \quad \mathbf{u}'(\mathbf{x}', \tau) = \mathbf{u}(\mathbf{x}, t). \tag{18), (19}$$

Thus the time derivative of the x_i component of velocity in the laboratory frame can be related to that in the moving frame via the chain-rule of differentiation:

$$\begin{aligned} \left.\frac{\partial u_i(\mathbf{x}, t)}{\partial t}\right|_{\mathbf{x}} &= \left.\frac{\partial x_j'}{\partial t}\right|_{\mathbf{x}} \left.\frac{\partial u_i'}{\partial x_j'}\right|_{\tau} + \left.\frac{\partial \tau}{\partial t}\right|_{\mathbf{x}} \left.\frac{\partial u_i'}{\partial \tau}\right|_{\mathbf{x}'} \\ &= -V_j \left.\frac{\partial u_i'}{\partial x_j'}\right|_{\tau} + \left.\frac{\partial u_i'}{\partial \tau}\right|_{\mathbf{x}'}. \end{aligned} \tag{20}$$

The quantity on the left-hand side of (20) is a variable measured by a velocity sensor fixed in the laboratory reference frame. If the magnitudes of the velocity fluctuations are small compared with the magnitude of $\mathbf{V}$ and if the time variation of the turbulent structure in the moving frame is small relative to the convective term, i.e. there is a 'frozen pattern', then the second term on the right side of (20) can be neglected with the result that

$$\left.\frac{\partial u_i}{\partial t}\right|_{\mathbf{x}} = -V_j \left.\frac{\partial u_i'}{\partial x_j'}\right|_{\tau}. \tag{21}$$

Strictly speaking, we cannot apply an order-of-magnitude analysis to estimate the terms on the right-hand side of (20) as they represent instantaneous values. In essence we must require that the characteristic time scale of the turbulent structure (or 'eddy') is long compared with the time it takes for the structure to be convected past a fixed point, i.e. the location of the velocity sensor. The characteristic dimension of the velocity sensor in the direction of $\mathbf{V}$ is assumed to be small compared with η.

If the convection velocity is equal to the mean velocity of the flow at point $\mathbf{x}$, then (21) becomes

$$\left.\frac{\partial u_i}{\partial t}\right|_{\mathbf{x}} = -\overline{U}_j \left.\frac{\partial u_i'}{\partial x_j'}\right|_{\tau}. \tag{22}$$

This is a somewhat different statement from (14) as it relates, in terms of spectra, the frequency spectrum in a fixed frame to a wavenumber spectrum in a reference frame moving at the convection velocity $\overline{\mathbf{U}}$. If the identity

$$\left.\frac{\partial}{\partial x_j'}\right|_{\tau} = \left.\frac{\partial}{\partial x_j}\right|_{t}$$

is used, (22) can be rewritten as

$$\left.\frac{\partial u_i}{\partial t}\right|_{\mathbf{x}} = -\overline{U}_j \left.\frac{\partial u_i}{\partial x_j}\right|_{t}, \tag{23}$$

where (19) has also been used. Note that if $\mathbf{V}$ is not steady then (19) is not valid.

Alternatively, one can transform the time derivative of the velocity fluctuations measured in the moving frame to the velocity derivatives in the fixed reference frame as

$$\left.\frac{\partial u_i'(\mathbf{x}', \tau)}{\partial \tau}\right|_{\mathbf{x}'} = \left.\frac{\partial x_j}{\partial \tau}\right|_{\mathbf{x}'} \left.\frac{\partial u_i}{\partial x_j}\right|_t + \left.\frac{\partial t}{\partial \tau}\right|_{\mathbf{x}'} \left.\frac{\partial u_i}{\partial t}\right|_{\mathbf{x}}$$

$$= V_j \left.\frac{\partial u_i}{\partial x_j}\right|_t + \left.\frac{\partial u_i}{\partial t}\right|_{\mathbf{x}}. \tag{24}$$

This relationship could be used to relate measurements made in a moving frame of reference to those in a fixed frame. The location of the velocity sensor is $\mathbf{x}' =$ constant in the moving frame or $\mathbf{x} = \mathbf{x}' + \mathbf{V}t$ in the fixed reference frame. In this case, if V_j is sufficiently large that the time-derivative term in the fixed frame can be neglected relative to the spatial-derivative product term then the result is

$$\left.\frac{\partial u_i'}{\partial \tau}\right|_{\mathbf{x}'} = V_j \left.\frac{\partial u_i}{\partial x_j}\right|_t. \tag{25}$$

Equations (22) and (25) express different relations and were derived under formally different assumptions.

There are numerous papers regarding Taylor's approximation, including those by Wills (1964), Favre (1965), Heskestad (1965) and a very comprehensive treatment by Lumley (1965). The interpretation of time spectra measured in high intensity turbulent flows is complex as Taylor's frozen-flow approximation is not valid in such a flow (Fisher & Davies 1964). Lumley (1965) developed a model to correct the high frequency portion of a spectrum for effects caused by deviations from Taylor's hypothesis. Lumley showed that, when certain criteria are satisfied, the main effect at high frequencies is that of a fluctuating convection velocity. That is, the high wavenumber isotropic regions are considered to be frozen and convected by a spatially uniform fluctuating velocity with the characteristics of the energy-containing eddies. The space and time scales of the convecting field are assumed sufficiently large compared with those of the high wavenumber convected field that the two are statistically independent. A criterion is formed which requires that intrinsic temporal changes in a framework moving with the mean velocity are small. The arguments used in formulating this criterion are particularly enlightening in interpreting the frozen-pattern assumption used in obtaining (21) for eddies of various sizes. Note that the convection velocity is now considered *unsteady* and equal to the mean velocity plus v_i, a temporally slowly varying quantity with a time scale very large compared with that of the high wavenumber structure and with a magnitude equal to that of the velocity scale of the energy-containing eddies. We shall let the magnitudes of the v_i be equal to those of the u_i, i.e. $\overline{v_1^2} = \overline{u_1^2}$, etc. Lumley's analysis leads to a relation between the measured and true one-dimensional spectra of the streamwise velocity fluctuations given by

$$F_1^m(k_1) = F_1(k_1) + \frac{\overline{u_1^2}}{2\overline{U}_1^2}(k_1^2 F_1'' + 4k_1 F_1' + 2F_1) - \frac{\overline{u_2^2} + \overline{u_3^2}}{\overline{U}_1^2}(k_1 F' + F_1), \tag{26}$$

where $F_1^m(k_1)$ is the value of the measured spectrum inferred from the frequency f using (15). A solution of (26) subject to the boundary conditions

$$\lim_{k_1 \to \infty} F_1(k_1) = \lim_{k_1 \to \infty} F_1'(k_1) = 0 \tag{27), (28}$$

was obtained by the present author and is given by

$$F_1(z) = \left|\left(1-\frac{b}{a}\right)^2 - \frac{4}{a}\right|^{-\frac{1}{2}} 2a^{-1}\int_{z_0}^{z} F_1^{(m)}(\xi)\exp\left\{\frac{1}{2}\left(\frac{b}{a}-3\right)(z-\xi)\right\} \times \sin\left\{\left|\left(1-\frac{b}{a}\right)^2 - \frac{4}{a}\right|^{\frac{1}{2}} \tfrac{1}{2}(z-\xi)\right\} d\xi \tag{29}$$

when $(1-b/a)^2 - 4/a < 0$. The variable $z = \ln k_1$ while a and b are defined by

$$a = \overline{u_1^2}/2\overline{U}_1^2, \quad b = (\overline{u_2^2}+\overline{u_3^2})/\overline{U}_1^2 \tag{30), (31}$$

and z_0 is determined by the value of $k_{1\infty}$ used to cut off the spectrum, i.e.

$$z_0 = \ln(c/\eta), \tag{32}$$

where c is a constant (a value of 3 was typically used). The inequality involving the coefficients of the differential equation is satisfied for all the flows to be considered here. The importance of correcting for deviations from Taylor's hypothesis in searching for universal shapes will be demonstrated later. The significance of similar corrections for various velocity-derivative statistics can be readily obtained from (26). Wyngaard & Pao (1972), noting that

$$\overline{\left(\frac{\partial^n u_1}{\partial x_1^n}\right)^2} = \int_0^\infty k_1^{2n} F_1(k_1)\, dk_1 \tag{33}$$

and

$$\frac{1}{\overline{U}^{2n}}\overline{\left(\frac{\partial^n u_1}{\partial t^n}\right)^2} = \int_0^\infty k_1^{2n} F_1^m(k_1)\, dk_1, \tag{34}$$

used (26) to obtain

$$\frac{1}{\overline{U}^{2n}}\overline{\left(\frac{\partial^n u_1}{\partial t^n}\right)^2} = \overline{\left(\frac{\partial^n u_1}{\partial x_1^n}\right)^2}\left[1+(2n^2-n)\frac{\overline{u_1^2}}{\overline{U}_1^2} + 2n\left(\frac{\overline{u_2^2}+\overline{u_3^2}}{\overline{U}_1^2}\right)\right]. \tag{35}$$

For $n = 1$, it is readily shown that

$$\epsilon_m = \epsilon\left[1+\frac{\overline{u_1^2}}{\overline{U}_1^2} + 2\frac{\overline{u_2^2}+\overline{u_3^2}}{\overline{U}_1^2}\right], \tag{36}$$

where ϵ_m denotes the measured value of the dissipation rate inferred from $\overline{(\partial u_1/\partial t)^2}$ using (8) and (14). Thus, if the turbulence intensities are of the order of 30 %, as is the case on the centre-line of an axisymmetric jet, then ϵ_m is 45 % too high.

An expression which is useful in correctly determining the right-hand side of (12) can be obtained by putting $n = 2$:

$$\frac{1}{\overline{U}_1^4}\overline{\left(\frac{\partial^2 u_1}{\partial t^2}\right)^2} = \overline{\left(\frac{\partial^2 u_1}{\partial x_1^2}\right)^2}\left[1+6\frac{\overline{u_1^2}}{\overline{U}_1^2} + 4\frac{\overline{u_2^2}+\overline{u_3^2}}{\overline{U}_1^2}\right]. \tag{37}$$

Using the definition of the normalized spectrum (1), along with (36) and (37), one can obtain

$$\frac{\int_0^\infty (\eta_m k_1)^4 \Phi_1^m(\eta_m k_1)\, d(\eta_m k_1)}{\int_0^\infty (\eta k_1)^4 \Phi_1(\eta k_1)\, d(\eta k_1)} = \frac{\left[1+6\frac{\overline{u_1^2}}{\overline{U}_1^2}+4\frac{\overline{u_2^2}+\overline{u_3^2}}{\overline{U}_1^2}\right]}{\left[1+\frac{\overline{u_1^2}}{\overline{U}_1^2}+2\frac{\overline{u_2^2}+\overline{u_3^2}}{\overline{U}_1^2}\right]^{\frac{3}{2}}}. \tag{38}$$

Φ_1^m and η_m refer to the measured values obtained from Taylor's approximation while Φ_1 and η refer to quantities obtained from Lumley's correction. Note that (38) gives the

ratio of the measured to the corrected skewness of $\partial u_1/\partial x_1$ if (12) is a good approximation for the flow field.

Another extension of Taylor's approximation for high intensity, high Reynolds number flows was proposed by Heskestad (1965). He used the relation

$$-\partial u_i/\partial t = U_j \partial u_i/\partial x_j, \tag{39}$$

where $U_j = \overline{U}_j + u_j$ and all derivatives are relative to a fixed reference frame. It should be noted that in this case the convection velocity is the instantaneous velocity in contrast to the previous derivation leading to (21). If (39) is applied to the u_1 component and the result is squared and averaged then, by use of the assumptions of independence of Fourier components with distant wavenumbers and local isotropy, (35) is obtained for $n = 1$. Similarly, the mean-square second derivative is given by

$$\overline{\left(\frac{\partial^2 u_1}{\partial t^2}\right)^2} = \overline{\left[U_k U_j \frac{\partial^2 u_1}{\partial x_k \partial x_j} + U_k \frac{\partial U_j}{\partial x_k}\frac{\partial u_1}{\partial x_j}\right]^2}, \tag{40}$$

which can be shown to reduce to (37) (see appendix). Thus Heskestad's corrections to the mean-square first and second derivatives of the streamwise velocity fluctuations agree with those given by Lumley's model. Wyngaard & Tennekes (1970) applied Heskestad's extension to show that the directly measured skewness of the time derivative of u_1 is related to the skewness of the spatial derivative of u_1 by

$$S\left(\frac{\partial u_1}{\partial t}\right) = S\left(\frac{\partial u_1}{\partial x_1}\right) \frac{[1 + 3\overline{u_1^2}/\overline{U}_1^2 + 2(\overline{u_2^2} + \overline{u_3^2})/\overline{U}_1^2]}{[1 + \overline{u_1^2}/\overline{U}_1^2 + 2(\overline{u_2^2} + \overline{u_3^2})/\overline{U}_1^2]^{\frac{3}{2}}}. \tag{41}$$

They also derived a relationship between the two kurtosis variables but much algebra and further assumptions were involved. For their curved mixing-layer flow, the corrections to the measured skewness and kurtosis values were less than 2 %. Note that (38) and (41) do not give the same correction to the skewness, but as different statistical quantities are corrected in each case this is not surprising.

Another problem in data analysis arises because of the dual sensitivity of the hot-wire anemometer to both velocity and temperature. As temperature and velocity fluctuations occur simultaneously in many flows, including geophysical flows, the measured hot-wire velocity signal is 'contaminated' by the concomitant temperature fluctuations. It is typically assumed that negligible contamination occurs when the overheat ratio a_w is of the order of 0·80, especially when the r.m.s. temperature fluctuations are of the order of 0·5 °C or less. This is not always a good assumption, and its validity depends on the velocity field statistic or cross velocity–temperature field statistic to be measured. Calibrations of the hot wires for our field experiments and some heated laboratory flows were carried out for the range of temperatures expected. The resulting hot-wire response equation for the velocity, temperature and linearizer-voltage fluctuations can be expressed as

$$e_L = \alpha u_1 - \beta\theta, \tag{42}$$

where

$$\alpha \equiv \left(\frac{\partial E_L}{\partial U_1}\right)_{T_c - T_a},$$

the velocity sensitivity in V $(\mathrm{m\ s^{-1}})^{-1}$, and

$$\beta \equiv (\partial E_L/\partial(T_c - T_a))_{U},$$

the temperature sensitivity in V °C^{-1}. Also, T_a is the mean ambient temperature, T_c is the calibration temperature and E_L is the linearizer output voltage. Now if it is assumed that the measured linearized signals are caused by velocity alone, then

$$e_L = \alpha u_{1m}. \tag{43}$$

Thus from (42) and (43),

$$u_{1m} = u_1 - \frac{\beta}{\alpha}\theta \tag{44}$$

and

$$\overline{u_{1m}^2} = \overline{u_1^2} - 2\frac{\beta}{\alpha}\overline{u_1\theta} + \frac{\beta^2}{\alpha^2}\overline{\theta^2} \tag{45}$$

on squaring and averaging. Similar reasoning applied to the derivative signal gives

$$\frac{\overline{\dot{u}_{1m}^2}}{\overline{\dot{u}_1^2}} = 1 - 2\frac{\beta}{\alpha}R_{\dot{u}_1\dot{\theta}}\left(\frac{\overline{\dot{\theta}^2}}{\overline{\dot{u}_1^2}}\right)^{\frac{1}{2}} + \frac{\beta^2}{\alpha^2}\frac{\overline{\dot{\theta}^2}}{\overline{\dot{u}_1^2}}, \tag{46}$$

where

$$R_{\dot{u}_1\dot{\theta}} \equiv \overline{\dot{u}_1\dot{\theta}}/[\overline{\dot{u}_1^2}\,\overline{\dot{\theta}^2}]^{\frac{1}{2}}. \tag{47}$$

The spectral analogue of (46) is

$$\frac{F_{\dot{u}_{1m}}}{F_{\dot{u}_1}} = 1 - 2\frac{\beta}{\alpha}\frac{F_{\dot{u}_1\dot{\theta}}}{F_{\dot{u}_1}^{\frac{1}{2}}F_{\dot{\theta}}^{\frac{1}{2}}}\left(\frac{F_{\dot{\theta}}}{F_{\dot{u}_1}}\right)^{\frac{1}{2}} + \frac{\beta^2}{\alpha^2}\frac{F_\theta}{F_{\dot{u}_1}}. \tag{48}$$

The co-spectrum $F_{\dot{u}_1\dot{\theta}}$ must be obtained with specially designed hot-wire and cold-wire double probes. The cold wire is placed within a Kolmogorov microscale of the hot wire so that simultaneous measurements of both field variables from effectively the same point in space are available. It should be pointed out, however, that the cold wire exhibits a finite velocity sensitivity, and [cf. (44)] one can write (Wyngaard 1971)

$$\theta_m = \theta - cu_1. \tag{49}$$

Thus measurements of cross-statistics are further contaminated and must be corrected. The double wire probes used in the experiments on the atmospheric surface layer were calibrated for both velocity and temperature sensitivity, so values of c have been determined for the cold wires. Estimates of the correction to $F_{\dot{u}_{1m}}$ were obtained from measurements of the ratio of the cospectra of $\dot{u}$ and $\dot{\theta}$, normalized by the square root of the spectral products. For $\eta k_1 > 0{\cdot}05$, the corrections to $F_{\dot{u}_{1m}}$ were less than 1 % and therefore neglected. It can be easily shown, however, that the value of $\overline{\dot{u}_{1m}\dot{\theta}_m}$, which should be zero by local isotropy, is completely dominated by the temperature-sensitivity contamination of the hot-wire signal for most measurements in the atmospheric surface layer.

A further consideration in examining the fine-scale velocity field data is possible wire-length attenuation effects. The spatial averaging effects of hot-wire anemometers has been extensively treated by Wyngaard (1968, 1969, 1971). Results are presented in terms of one-dimensional spectra and are quite useful for estimating wire-length attenuation effects.

All the above corrections were estimated and taken into account to establish confidence limits on our universal spectral shapes and the values of any estimated statistics relating to local isotropy. The data to be considered in this paper are defined in table 1.

Flow	R_λ	x/d	y/d	f_c/f_k	η/l_{wire}	Remarks	Reference
Isotropic grid flow	41	120†	—	—	$\sim$ 1·0	Re_M = 17000	Comte-Bellot & Corrsin (1971)
	65	98†	—	—	$\sim$ 1·0	Re_M = 34000	
Homogeneous shear flow	130	10·5‡	0·50‡	—	$\sim$ 1·0	—	Champagne *et al.* (1970)
Two-dimensional cylinder wake flow	88	299	0·0	6·0	1·93	Re_d = 5080	Present study
	138	299	0·0	2·0	1·14	Re_d = 10000	
	182	299	0·0	1·0	0·81	Re_d = 19050	
Axisymmetric jet	626	70	0·0	2·25	0·44	$Re_d = 3{\cdot}7 \times 10^5$	Present study
Laboratory boundary layer	411	z = 0·3 m		1·5	0·34	IMST wind tunnel§	Mestayer (1975)
Atmospheric boundary layer over land	2800	5 m < z < 23 m		2·5	0·58	Averaged over eight 15 min runs	Wyngaard & Pao (1972)
	850	z = 2·00 m		1·35	0·39	234 s of data	Williams (1974)
	7000	z = 4·09 m		1·42	0·66	15 min of data	Champagne *et al.* (1977)
	13000	z = 56 m		1·41	0·82	Averaged over two 20 min runs	Present study

† $t\bar{U}/M$, where M = mesh size; ‡ x/h, y/h, where h = tunnel height; § x = 34 m, $z/\delta \approx 0{\cdot}3$, $\bar{U}$ = 7 m/s.

TABLE 1

Much of the data obtained from various investigators were eliminated from consideration on the basis of the following points:

(i) spatial resolution of probes much greater than η;

(ii) spatial resolution of non-cylindrical sensors not well defined;

(iii) inadequate sampling time resulting in an inordinate amount of scatter;

(iv) low-pass filter setting f_c, used to avoid aliasing, equal to or less than f_k, defined as $f_k = \overline{U}_1/2\pi\eta$.

High-quality spectral data were necessary for this study as the second and fourth moments of the spectra were required out to about a Kolmogorov normalized wavenumber of unity. When the cross-component velocity spectra were also available, the relationships between the measured component spectra were compared with (9) and (10) to determine if inertial and/or dissipative local isotropy existed. Values of the kinematic viscosity of air for the various data sets were obtained from appendix 1 of Batchelor (1967).

4. Experimental arrangement

As much of the data to be considered are those of the present author, primarily because the experiments were designed specifically to obtain measurements of the fine-scale structure of turbulent velocity fields, a description of the experimental facilities used will be presented. For any details of the experiments in the other works cited, the reader will have to refer to the appropriate reference given.

4.1. *The axisymmetric jet*

A 7·5 h.p. centrifugal blower supplied the air flow through a preliminary calming box, consisting of screens and a honeycomb, to a diffuser and then to a plenum chamber of diameter 30 in. The plenum chamber contained two screens to reduce the turbulence level at the nozzle exit. The air was exhausted through a nozzle with a diameter of 4 in. and a contraction ratio of 56:1. Before passing to the blower, the air was initially cooled by two air conditioners and cleaned using two Farr HP 100 filters. The temperature of the jet at the nozzle exit could be maintained to within 4 °F of ambient room temperature, and the latter did not vary more than 2 °F during the entire day. As all measurements were carried out at $x/d > 50$, the temperature was sufficiently close to ambient and sufficiently constant that no corrections were required. The jet facility was mounted horizontally with the centre-line of the jet 6 ft above the laboratory floor. This height, as well as the size of the laboratory room, determined the maximum usable downstream distance allowable before any distortion of the jet occurred. This value is equivalent to $x/d \approx 80$. The maximum speed attainable at the nozzle exit was 86 m/s, although most measurements were carried out with an exit velocity of 54 m/s, or a Reynolds number of $3{\cdot}7 \times 10^5$.

Measurements were restricted to the jet centre-line in the region $50 \leqslant x/d \leqslant 70$. Although it was desirable to carry out the measurements at the highest possible Reynolds number, important considerations such as the ratio of Kolmogorov's length scale to the wire length l_w and the maximum sampling rate of the analog-to-digital converter had to be taken into account. The variation of Kolmogorov's length scale as a function of x/d and the Reynolds number $Re = U_0 d/\nu$, where U_0 is the nozzle exit

speed and d the nozzle diameter, was determined experimentally. From these results, it was decided to carry out the measurements at $x/d = 70$, where the resulting length ratio η/l_w was 0·44. The actual wire length used was 0·37 mm and the diameter was about 2·3 μm. From Wyngaard's (1968) wire-length attenuation calculations, the measured one-dimensional spectrum should be underestimated by of the order of 10 % at $k_1 l_w = 2$ and 20 % at $k_1 l_w = 4$. This is within the statistical uncertainty or scatter in the data at these large wavenumbers and all the data fall below $k_1 l_w = 4$. Wyngaard's analysis is based on Pao's (1965) spectral form with a value of Kolmogorov's universal constant of 1·7. Wyngaard & Pao (1971) have shown that this spectral form is not adequate, especially in the high wavenumber region, but it may at least give a reasonable estimate for the wire-length attenuation predictions (Champagne, Wygnanski & Pao 1976). Further, the jet spectral data must be corrected for effects caused by deviations from Taylor's hypothesis using Lumley's model and this results in corrections larger than 20 % beyond $\eta k_1 = 0{\cdot}5$. Thus although the jet data must be considered with some reservation, they were obtained to provide information on high Reynolds number fine-scale structure under controlled laboratory conditions.

4.2. *The low-speed wind tunnel*

The turbulent wake studies were performed in a new closed-return wind tunnel with a contraction ratio of 10 : 1 and a free-stream turbulence intensity of 0·05 %. The test section is rectangular in cross-section (2 × 3 ft) and 20 ft in length. The top and bottom walls of the test section are mounted on jacks to provide a controlled divergence of each wall for establishing pressure gradients. For the wake studies, a slight divergence of the walls was used to compensate for boundary-layer growth and gave, effectively, a zero pressure gradient. Polished stainless-steel cylinders with diameters ranging from 0·375 in. to 1·50 in. were used to generate the wake flows. The cylinders were mounted a few inches downstream of the test section inlet. The angularity of the flow near the test-section inlet was virtually undetectable, i.e. less than 0·1° with respect to the axis of the test section, except in the wall boundary layer. Air temperature was monitored with a thermistor probe with an accuracy of $\pm$ 0·1 °F and the air temperature could be controlled to within $\pm$ 0·3 °F of the calibration value by using a water-cooled heat exchanger mounted downstream of the axial flow blower.

Most of the spectral measurements were carried out on the wake centre-line at $x/d = 299$ for a Reynolds number based on the cylinder diameter and free-stream velocity of 19050. At this Reynolds number, η/l_w was 0·73 at $x/d = 299$ and the turbulence Reynolds number was 182. Higher Reynolds numbers were not used to avoid wire-length attenuation problems.

4.3. *Laboratory instrumentation*

Velocity fluctuations were measured with Disa type 55D01 constant-temperature anemometers in conjunction with Disa type 55D10 linearizers. The linearizers were calibrated to known flow conditions in the wind-tunnel test section or in the free-stream flow of the mixing-layer facility. An overheat ratio of 0·7–0·8 was used for all wires. Lateral-component fluctuations were measured with a symmetric X-array and the lateral-component sensitivities were obtained by yawing the probe $\pm 5°$ in the plane parallel to that of the two wires. The single and X-array hot-wire probes were

constructed from 2·3 μm tungsten wire which was copper/gold plated. The active, or unplated, portion of the wires was about 0·4 mm in length and located at the geometrical centre of the whole wire. Typically, the distance between support stems was 3 mm to avoid support-stem flow-field disturbances. For X-wire probes, the wires were separated by about 0·4 mm, or one (active) wire length, a value chosen with Wyngaard's (1968) results in mind. The length 0·4 mm corresponds to a length-to-diameter ratio of 175, the minimum value of this ratio required to keep a reasonably uniform temperature distribution (Champagne *et al.* 1967). The velocity fluctuation signals were differentiated using an analog circuit which consisted of a Philbrick P65AU operational amplifier used as a follower, a Philbrick/Nexus Model 1003 FET operational amplifier used as a differentiator, and two Krohn-Hite Model 330 band-pass filters. One filter was placed at the circuit input to eliminate the high frequency noise from the anemometer and linearizer before differentiation and the other at the circuit output to improve the signal-to-noise ratio and to minimize aliasing. Care was taken to avoid phase shift and amplitude distortion of the signal wave forms. The time constant of the differentiator was changed for each experiment to optimize the signal-to-noise ratio in the frequency band of interest. The total phase shift of the various differentiator circuits was quite linear with frequency over the band of interest and typically the overall signal-to-noise ratio was about 20:1.

Nearly all signal processing was carried out using a direct on-line computer system. The digital data acquisition system is described in detail in Champagne *et al.* (1976).

Spectral measurements were obtained by means of the fast Fourier transform (Pao, Hansen & MacGregor 1969). The continuous signals were converted to digital samples with a resolution of 14 bits plus a sign bit and the maximum sampling rate was 18000 s^{-1}. The samples were processed in ensembles of 8192, dictated by computer memory requirements, and typically 300 ensembles or $2{\cdot}5 \times 10^6$ samples were processed to ensure convergence of the ensemble means, which was monitored through intermediate print-outs. Spectral windows of 0·10 and 2·18 Hz were used: the 0·10 Hz window was used to resolve the large-scale turbulence and these results overlapped with the broad-band spectra obtained with the 2·18 Hz window. Analog checks of several spectral points fell within $\pm$ 10 % of the digital values. Also, the root mean squares of the fluctuating signals were determined both from the spectrum and by the usual analog method and the results always agreed to within a few per cent. Higher-order spectra were measured in the same manner as above, except that the digitized samples were raised to the appropriate power in the computer before fast Fourier transforming.

The velocity spectra were effectively prewhitened after being sampled by the use of transversal filtering. The main purpose of prewhitening after the data have been obtained in digital form is to avoid difficulty with the minor lobes of the spectral windows, commonly referred to as 'spectral leakage'. The result of this leakage problem is to distort the high frequency end of the spectra where the spectral values are five or six orders of magnitude below that of the large-scale energy-containing region. One way of circumventing this problem is to measure the spectrum of the time derivative of the signal (non-prewhitened) and then compute the spectrum of the signal itself from the appropriate identity relating the two. This was carried out for the high Reynolds number jet: the results from the measured prewhitened velocity spectrum were compared with the measured (non-prewhitened) velocity-derivative spectrum and excellent agreement was found. The same comparison without prewhitening the

velocity spectrum indicated that the spectral estimates in the high frequency tails were considerably overestimated by spectral leakage.

The hot wires were normally calibrated directly on-line to determine the overall gain of the system. Wherever feasible, the overall on-line system and programs were checked with known signals. Free-stream spectra for all types of signals considered, i.e. first- and higher-order spectra of the velocity fluctuations and their derivatives, were obtained to determine relevant noise levels in the data.

4.4. *Field sites*

The results from two of our own field experiments will be presented. The first of these, labelled GUMBO, was performed in co-operation with the Air Force Cambridge Research Laboratories at their site in Minnesota. This was a completely instrumented and documented site with the field upwind of the towers specially prepared to provide a uniform and known surface roughness. Details of this experiment are discussed thoroughly in Champagne *et al.* (1977). Our second experiment was performed in conjunction with the Danish Atomic Energy Commission, RISØ, at their 130 m tower site in Roskilde, Denmark. The probes were located at an elevation of 56 m. The special double wire probes, one hot wire and one cold wire, were used in this experiment. Because of long cable lengths between sensors and electronics and relatively low signal levels, difficulty with 50 Hz line noise pick-up was encountered and the spectral data required noise correction. This was carried out, but as the line pick-up problem was present in the noise data also, we must assign some degree of uncertainty to the corrected data. It is difficult to give precise estimates of the uncertainty, but the high wavenumber portions ($\eta k_1 > 0{\cdot}7$) of the spectra are probably consistently low because of the correction. These data are referred to as FS II or Fine Structure II.

4.5. *Field-experiment instrumentation*

Two channels of Disa 55M01 constant-temperature anemometers and Disa 55D10 linearizers were used for velocity measurements. The hot wires used were either 0·4 mm long and 2·3 μm in diameter or 1·25 mm long and 5 μm in diameter. An EG&G Model 198 three-component sonic anemometer and associated read-out circuitry were used to provide velocity-component measurements from d.c. to 10 Hz, which provides an overlap with the hot-wire results (d.c. to the Kolmogorov frequency, about 2 kHz). The sonic anemometer is an absolute instrument and thus permits an *in situ* check on the hot-wire calibration. The path length or spatial resolution of the sonic anemometer is 20 cm. A small low turbulence intensity calibration facility was designed and constructed so that the hot-wire probes could be calibrated at the field site before and after each data run. The temperature of the calibration stream can be controlled through use of a small radiator which is cooled using water from a constant-temperature bath. The hot wires were therefore calibrated over the required temperature and velocity range. An MKS Baratron pressure transducer system is used for calibration of air pressure measurements. Relevant noise levels in the data were obtained by placing the hot wire in the low intensity calibration tunnel when it was operating at a speed nearly equal to the mean speed for the data obtained. The noise signal was passed through the same processing circuits as the actual data and recorded on the analog tape recorder. A Hewlett-Packard Model 2801A quartz thermometer was used for mean and calibration temperature measurements. Specially designed

sensitive a.c. bridges and 0·625 μm diameter platinum cold wires were used for fluctuating temperature measurements. Krohn-Hite 3342R filters, differentiator circuits, prewhitening and buck-and-gain circuits were used to condition the signals before recording. A Honeywell Model 7600 fourteen-channel analog tape recorder or a Hewlett-Packard Model 3960 four-channel tape recorder was used for recording analog tapes. The analog tapes were appropriately digitized using one of our analog-to-digital conversion systems. A complete discussion of the digital data analysis for the field experiments is presented by Champagne *et al.* (1977).

5. Results and discussion

5.1. *Low Reynolds number spectra*

The one-dimensional energy spectra are $F_1(k_1)$, $F_2(k_1)$ and $F_3(k_1)$, whose integrals over all wavenumbers are $\overline{u_1^2}$, $\overline{u_2^2}$ and $\overline{u_3^2}$, respectively. Taylor's approximation in the form $k_1 = 2\pi f/\overline{U}_1$ was used to transform the frequency f to the wavenumber k_1, the x_1 component. x_1 is the co-ordinate in the direction of the mean flow, x_2 is that in the direction of the mean velocity gradient and x_3 is the co-ordinate perpendicular to the x_1, x_2 plane. Unless designated otherwise, the spectra are presented here in Kolmogorov-normalized form, i.e. divided by $(\epsilon\nu^5)^{\frac{1}{4}}$ as indicated by (1). The value of the dissipation rate ϵ was estimated from the second moment of the dimensional spectra using the assumption of dissipative local isotropy, or

$$\epsilon = 15\nu \int_0^\infty k_1^2 F_1(k_1)\, dk_1. \tag{50}$$

Figure 1 shows the low R_λ spectra obtained in several flow fields. The spectra collapse together for $\eta k_1 > 0{\cdot}1$, whereas significant differences occur in the lower wavenumber range. The solid straight line indicates a slope of $+\frac{1}{3}$, which is the slope predicted for an inertial subrange, although the R_λ values are probably not large enough to permit the existence of inertial local isotropy. As R_λ increases, however, the lower *normalized* wavenumber components increase in spectral content, apparently developing towards inertial-subrange behaviour. Of the flows considered in figure 1, the homogeneous shear flow approaches the $+\frac{1}{3}$ slope most closely but only over a very narrow wavenumber range. One requirement for local isotropy is that the dissipative spectral region be at wavenumbers considerably larger than those at which turbulent energy production occurs. Figure 2 presents the turbulent energy production and viscous dissipation spectra for the homogeneous shear flow in the forms $k_1 F_{12}(k_1)\, \partial\overline{U}_1/\partial x_2$ and $15\nu k_1^3 F_1(k_1)$, respectively, where

$$-\overline{u_1 u_2}\frac{\partial \overline{U}_1}{\partial x_2} = \frac{\partial \overline{U}_1}{\partial x_2}\int_0^\infty k_1 F_{12}(k_1)\, d(\ln k_1) \tag{51}$$

and

$$\epsilon = 15\nu \int_0^\infty k_1^3 F_1(k_1)\, d(\ln k_1). \tag{52}$$

A reasonable measure of the wavenumber region characterized by turbulent energy production is the first moment of the shear-stress spectrum, or

$$k_p \equiv \int_0^\infty k_1 F_{12}(k_1)\, dk_1 \Big/ \int_0^\infty F_{12}(k_1)\, dk_1. \tag{53}$$

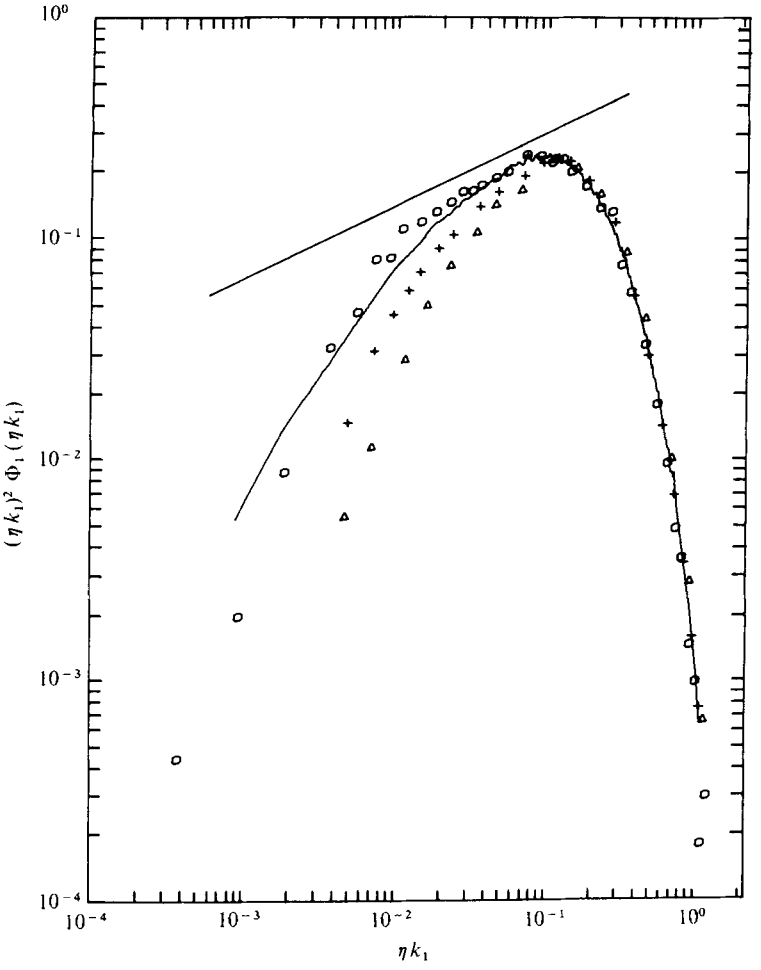

FIGURE 1. Second moments of low Reynolds number normalized spectra. ——, cylinder wake flow, $R_\lambda = 138$; △, CBC (Comte-Bellot & Corrsin 1971) grid flow, $R_\lambda = 41$; +, CBC grid flow, $R_\lambda = 65$; ○, CHC (Champagne, Harris & Corrsin 1970) homogeneous shear flow, $R_\lambda = 130$. Solid straight line has a slope of $+\frac{1}{3}$.

The Kolmogorov wavenumber is 28 cm^{-1} and k_p is 0·4 cm^{-1}, so $k_K/k_p \approx 70$. Champagne *et al.* (1970), on the basis of this result and spectral transfer time arguments, indicated that their flow could not be expected to exhibit an inertial subrange but that the flow is probably locally isotropic in the dissipation wavenumber region. Table 2 presents results of the streamwise-derivative tests of local isotropy based on (7). Although results are not presented for the $R_\lambda = 138$ wake case, examination of the normalized spectra indicates that no significant difference should be expected from the $R_\lambda = 182$ data. Thus, as the latter appear to show reasonable agreement with the streamwise-derivative equalities required for local isotropy, the $R_\lambda = 138$ wake flow is assumed locally isotropic, at least in the dissipative wavenumber region. The Comte-Bellot & Corrsin (1971) grid flow is also assumed locally isotropic on the basis of the observed agreement with the Kármán–Howarth (1938) relation between transverse

Flow	R_λ	$\overline{\left(\frac{\partial u_1}{\partial x_1}\right)^2}\Big/\overline{\left(\frac{\partial u_2}{\partial x_1}\right)^2}$	$\overline{\left(\frac{\partial u_2}{\partial x_1}\right)^2}\Big/\overline{\left(\frac{\partial u_3}{\partial x_1}\right)^2}$	$S\left(\frac{\partial u_1}{\partial x_1}\right)$	$S\left(\frac{\partial u_2}{\partial x_1}\right)$	$S\left(\frac{\partial u_3}{\partial x_1}\right)$	$K\left(\frac{\partial u_1}{\partial x_1}\right)$	$K\left(\frac{\partial u_2}{\partial x_1}\right)$	$K\left(\frac{\partial u_3}{\partial x_1}\right)$
Homogeneous shear flow	130	0·55	1·04	—	—	—	—	—	—
Two-dimensional cylinder wake flow	182	0·58	0·97	−0·48	0·028	0·028	5·7	7·6	7·9
Axisymmetric jet	626	0·70† 0·63‡	—	−0·67† −0·68‡	0·024	—	14·0	21·6	—
Atmospheric boundary layer over land, GUMBO	7000	—	—	−0·74 to −0·80	—	—	27·0	—	—
Atmospheric boundary layer over land, FS II	13000	—	—	−0·96	—	—	38·0	—	—

† Ratio directly from time-derivative measurements.
‡ Corrected for effects caused by deviations from Taylor's approximation.

TABLE 2

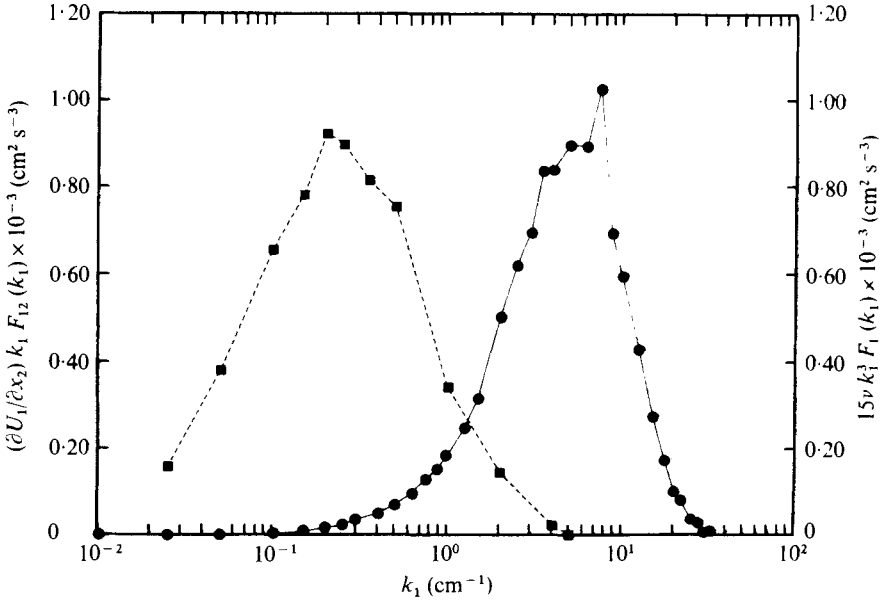

FIGURE 2. Spectral distributions of turbulent production and viscous dissipation rates for homogeneous turbulent shear flow.

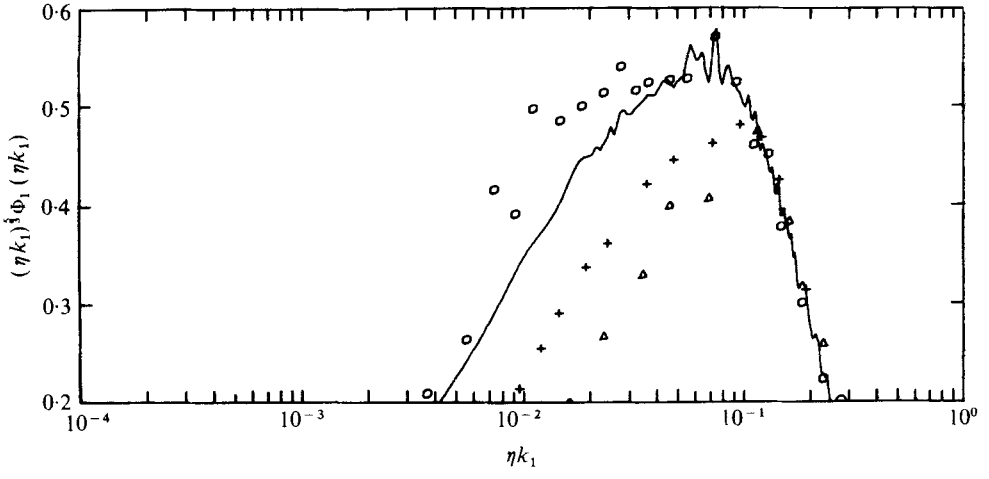

FIGURE 3. Low Reynolds number universal constant. ——, cylinder wake, $R_\lambda = 138$; △, CBC grid flow, $R_\lambda = 41$; +, CBC grid flow, $R_\lambda = 65$; ○, CHC homogeneous shear flow, $R_\lambda = 130$.

and longitudinal correlations and the fact that the dissipation rate obtained from the actual energy decay rate agrees closely with that obtained from (50).

Closer examination of the low R_λ spectral data can be achieved by plotting

$$(\eta k_1)^{\frac{5}{3}} \Phi_1(\eta k_1) \quad vs. \quad \eta k_1$$

on linear–log paper as shown in figure 3. If an inertial subrange exists, this is equivalent to plotting α_1 *vs.* ηk_1 according to Kolmogorov's second hypothesis, and through the

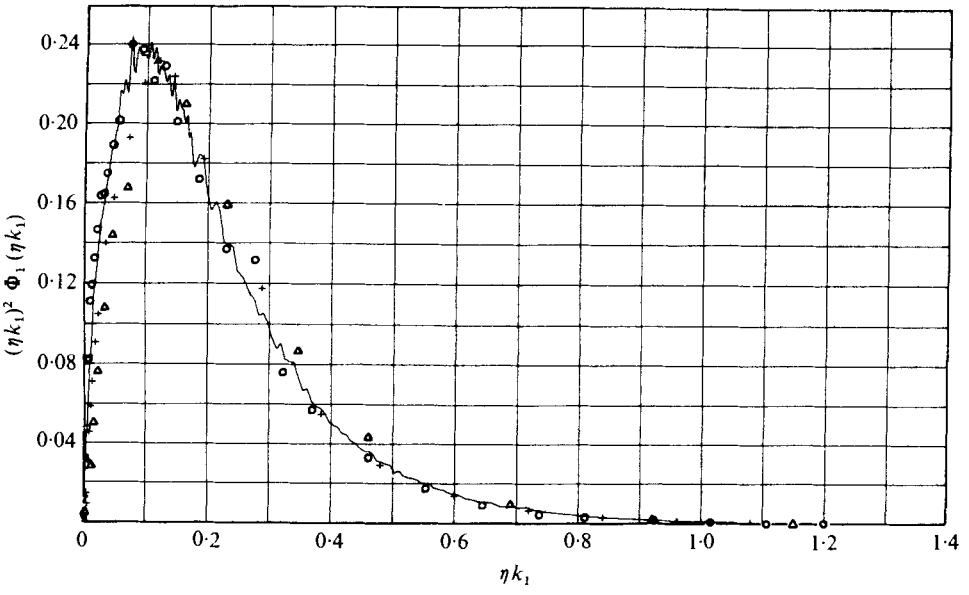

FIGURE 4. Second moments of the low Reynolds number normalized spectra. ——, cylinder wake flow, $R_\lambda = 138$; △, CBC grid flow, $R_\lambda = 41$; +, CBC grid flow, $R_\lambda = 65$; ○, CHC homogeneous shear flow, $R_\lambda = 130$.

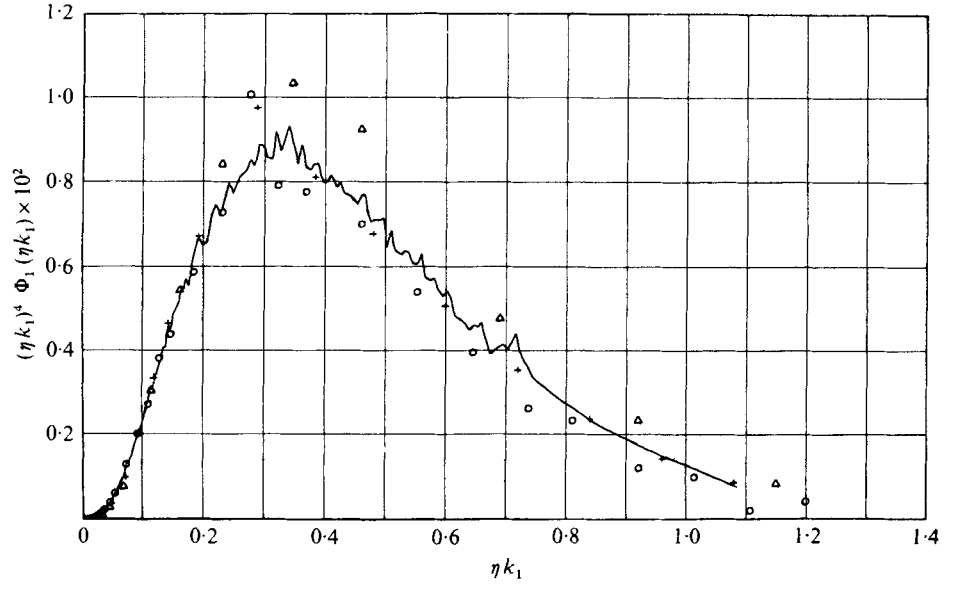

FIGURE 5. Fourth moments of low Reynolds number normalized spectra. ——, cylinder wake flow, $R_\lambda = 138$; △, CBC grid flow, $R_\lambda = 41$; +, CBC grid flow, $R_\lambda = 65$; ○, CHC homogeneous shear flow, $R_\lambda = 130$.

inertial-subrange region a line fit to the data should have zero slope. It is evident that no inertial subrange exists for these low R_λ turbulent flow fields. Figure 4 is a linear plot of $(\eta k_1)^2 \Phi_1(\eta k_1)$ *vs.* ηk_1. The second moments of the spectra exhibit peak values of 0·24, which occur at $\eta k_1 \approx 0{\cdot}10$ for the sheared flows and at a slightly higher wavenumber, about $\eta k_1 \approx 0{\cdot}12$, for the non-sheared grid flows. The data of Stewart & Townsend (1951) and Kistler & Vrebalovich (1966) on non-sheared grid flows also show that the peak occurs at $\eta k_1 \approx 0{\cdot}12$. The spectral region where both inertial transfer and viscous effects are important appears to be roughly $0{\cdot}05 \leqslant \eta k_1 \leqslant 1$. The fourth moments of the spectra, shown in figure 5, demonstrate how closely the spectra collapse together in the high wavenumber region. This indicates that the fine-scale structure of the different flow fields is similar at least for the R_λ range presented here, viz. 40–138. Although Kolmogorov scaling appears to be applicable for these low R_λ values, the entire form of the spectrum could change as R_λ increases to some sufficiently large value and then remains universal as required by the original Kolmogorov hypothesis. If the normalized spectral shape does not attain a universal form, but rather varies continuously with R_λ, this would be consistent with the modified hypothesis. The fourth-moment curves have peak values of about $9{\cdot}9 \times 10^{-3}$, occurring at $\eta k_1 \sim 0{\cdot}3$–$0{\cdot}35$. No data on the skewness of $\partial u_1/\partial x_1$ are available for most of these flows. The normalized spectral results for the $R_\lambda = 88$ cylinder wake flow are essentially identical to the above.

Figures 6–8 show the u_2 and u_3 spectra, which in normalized form are $\Phi_2(\eta k_1)$ and $\Phi_3(\eta k_1)$, for the homogeneous shear flow. Also shown in the figures by a solid line is a curve computed from the measured u_1 spectrum using the isotropic relation (9). The computed curve is in fair agreement with the measured spectra although it tends to be high at larger ηk_1. As shown in table 2, the isotropic equations relating the streamwise derivatives were found to be a good approximation for this flow. Further, from spatial correlation measurements, the results

$$\overline{\left(\frac{\partial u_1}{\partial x_1}\right)^2} \Big/ \overline{\left(\frac{\partial u_1}{\partial x_2}\right)^2} = 0{\cdot}52, \quad \overline{\left(\frac{\partial u_1}{\partial x_1}\right)^2} \Big/ \overline{\left(\frac{\partial u_1}{\partial x_3}\right)^2} = 0{\cdot}58$$

were obtained. Thus the results for homogeneous shear flow appear to be consistent with dissipative local isotropy. Further evidence against the existence of an inertial subrange in this flow is presented in figure 9, which shows

$$0{\cdot}75(\eta k_1)^{\frac{5}{3}} \Phi_i(\eta k_1), \quad i = 2, 3.$$

Very similar results were obtained for the $R_\lambda = 182$ wake flow. Figure 10 shows the fourth-moment results for the Φ_1 spectra obtained from different straight hot wires and an X-wire array. The spectral levels for normalized wavenumbers greater than 0·4 are consistently slightly higher than those shown in figure 4, even considering the inevitable scatter in the data. The squares represent results for which the wire was 0·37 mm long, f_c/f_k was 1·04 and the data were noise corrected in the mean square by subtracting off the background noise level from the entire system, determined by placing the hot wire in the free stream and running the tunnel at the corresponding mean speed. The dotted data were taken with a wire 0·4 mm long with $f_c/f_k = 0{\cdot}80$, and no noise correction was applied. The solid line represents data from an X-wire array where the wire length was 0·42 mm and the wire separation was about 0·4–0·5 mm. This plot indicates the degree of statistical scatter and the reproducibility

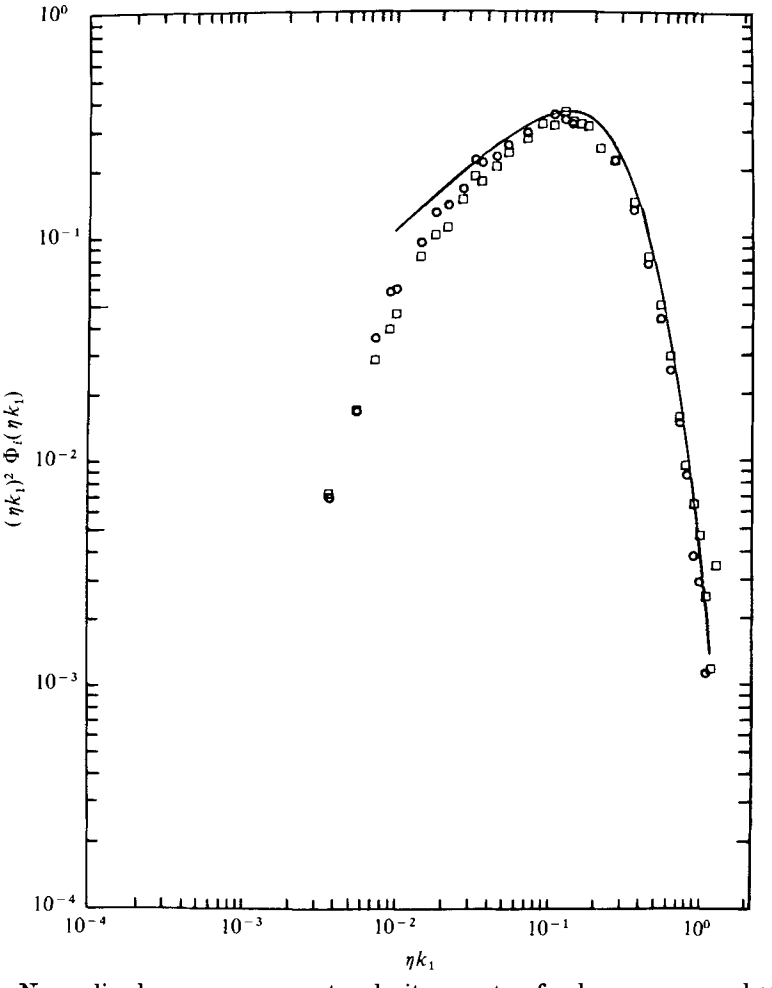

FIGURE 6. Normalized cross-component velocity spectra for homogeneous shear flow. □, u_2 spectrum; ○, u_3 spectrum; ——, computed spectrum.

achieved, gives a check on the spatial resolution of the X-wire array, and provides some confidence in the calibration technique for the X-wire array. The skewness obtained by determining the area under the data after an extrapolation of the tail to zero and then using (12) was $-0{\cdot}64$. The extrapolation was carried out using a ninth-order least-squares polynomial fit to the noise-corrected straight-wire data. Least-squares polynomial fits of the form

$$\ln F_1(k_1) = B_1 + B_2 x + B_2 x^2 + \ldots + B_{n+1} x^n \tag{54}$$

were used, where $x = \ln(\eta k_1)$ or $\ln k_1$. The directly measured value obtained from sampling the derivative signal, determining the moments and averaging was $-0{\cdot}48$. If the directly measured value is correct, this is a difference of 33 % which is not attributable to deviations from Taylor's hypothesis, to 'leakage' problems from the window tails as the data were digitally prewhitened, nor predominantly to effects caused by the lack of perfect local isotropy of the flow field. The difference is probably

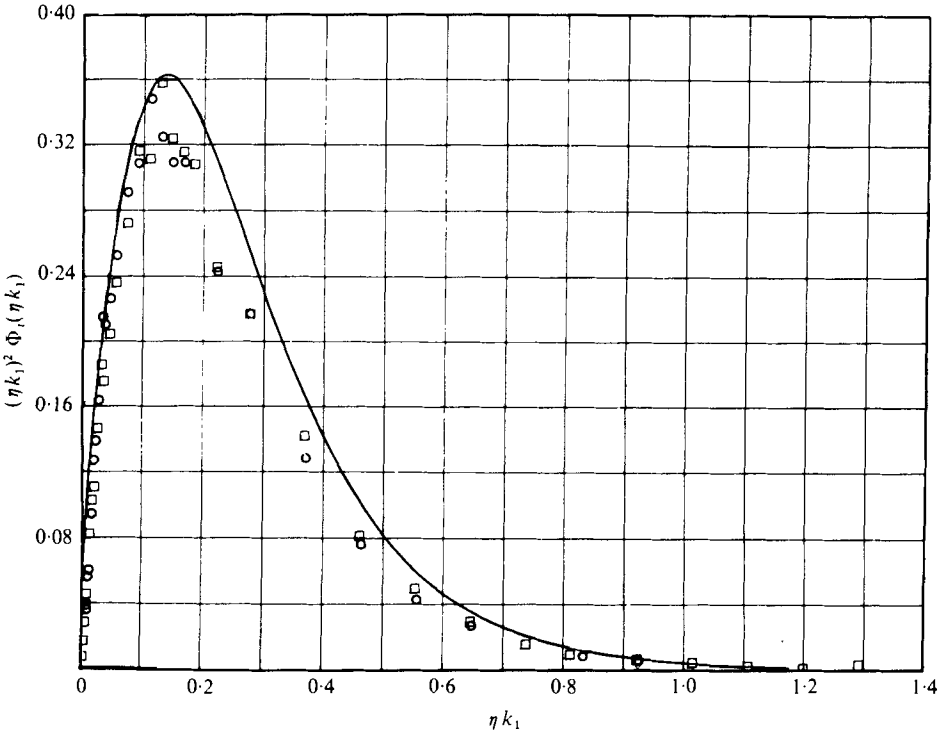

FIGURE 7. Normalized cross-component velocity spectra for homogeneous shear flow. □, u_2 spectrum; ○, u_3 spectrum; ——, computed spectrum.

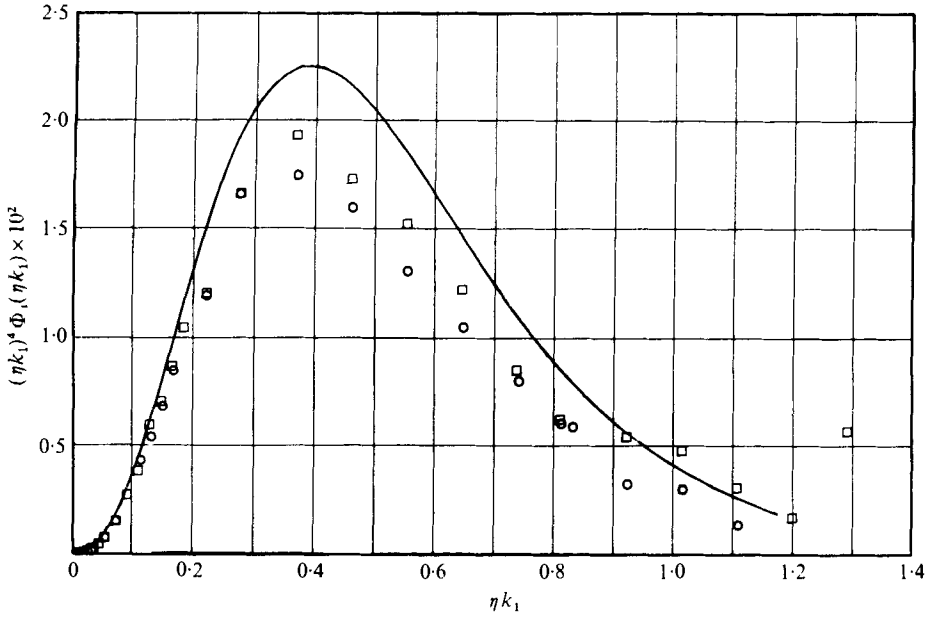

FIGURE 8. Normalized fourth moments of cross-stream velocity spectra for homogeneous shear flow. □, u_2 spectrum; ○, u_3 spectrum; ——, computed spectrum.

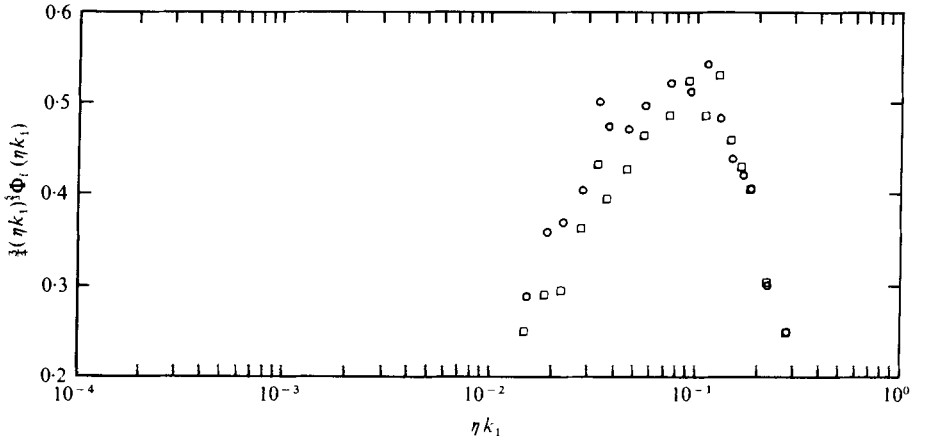

FIGURE 9. Universal constant from cross-stream velocity spectra for homogeneous shear flow. □, u_2 data; ○, u_3 data.

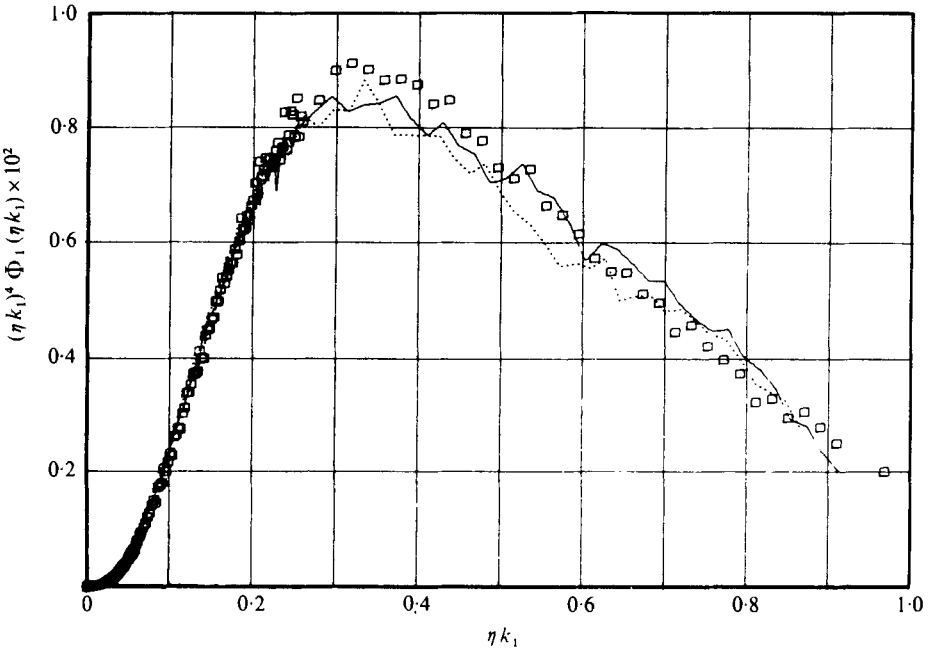

FIGURE 10. Normalized fourth moments of one-dimensional spectra for $R_\lambda = 182$ cylinder wake flow. □, single wire, $l = 0{\cdot}37$ mm; ···, single wire, $l = 0{\cdot}4$ mm; ——, X-wire, $l = 0{\cdot}42$ mm.

a result of the Reynolds number being too low for (11) to be a good approximation. Perhaps the difference is a crude measure of how close to 'sufficiently high Reynolds number' a given flow is. Further checks on local isotropy are presented in figures 11–13. The solid line in the figures is the curve computed from the measured u_1 spectrum using the isotropic relation (9). The computed curve is in fair agreement with measured spectra but is again consistently higher than the measured spectra in the larger wave-number region. The equalities (7) are reasonably satisfied as shown in table 2. The

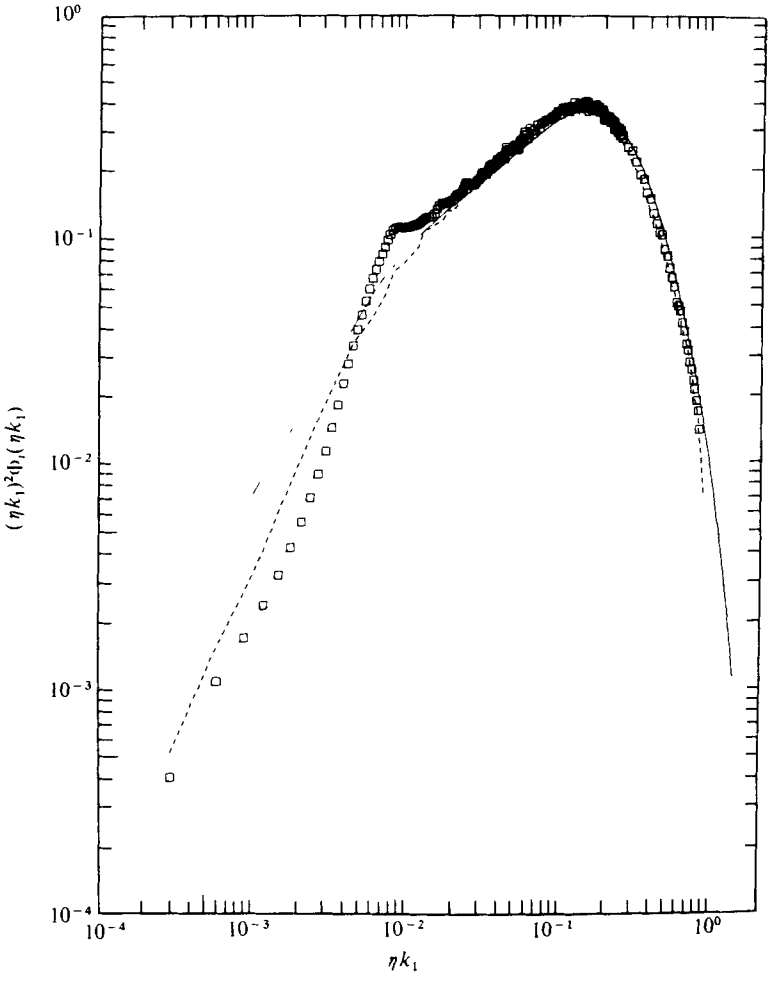

FIGURE 11. Normalized cross-component velocity spectra for two-dimensional wake flow; $R_\lambda = 182$. □, u_2 spectrum; – – –, u_3 spectrum; ——, computed spectrum.

curious bump in the u_2 spectrum occurs at a Strouhal number in the region of 0·08 and is similar to that observed by Uberoi & Freymuth (1969), who found a bump at a Strouhal number of about 0·09. Their data were obtained at $Re = 2160$ and $x/d = 200$. The spectral bump is illustrated again in figure 14, which shows the dimensional wake spectra. These low Strouhal number peaks differ from the classical result of 0·21 for the same Reynolds number range, but this value was obtained from measurements very close to the cylinder, typically $x/d < 10$ (Roshko 1960). k_K is just $1/\eta$.

5.2. *Turbulent jet spectra and Lumley's correction*

Laboratory flows with Kolmogorov microscales of the order of 0·5–1 mm (reasonable wire lengths) seem to be limited to R_λ values of around 10^3. The laboratory flow most commonly used to obtain large R_λ values is an axisymmetric free jet issuing into quiescent surroundings. As the length scales, including η, increase linearly with distance from the source in a round jet, this permits the possibility of moving downstream

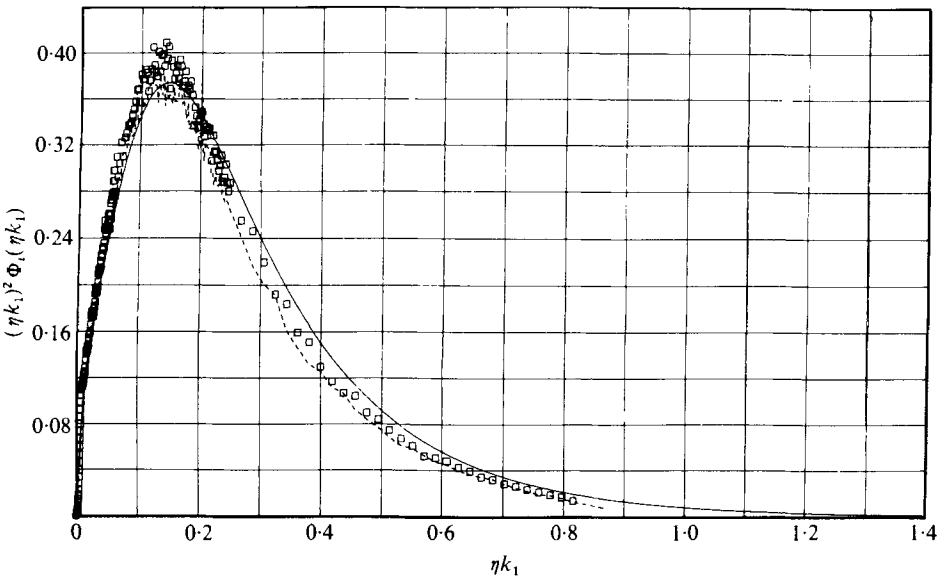

FIGURE 12. Normalized second-moment spectra of wake flow. □, u_2 spectrum; – – –, u_3 spectrum; ——, computed spectrum.

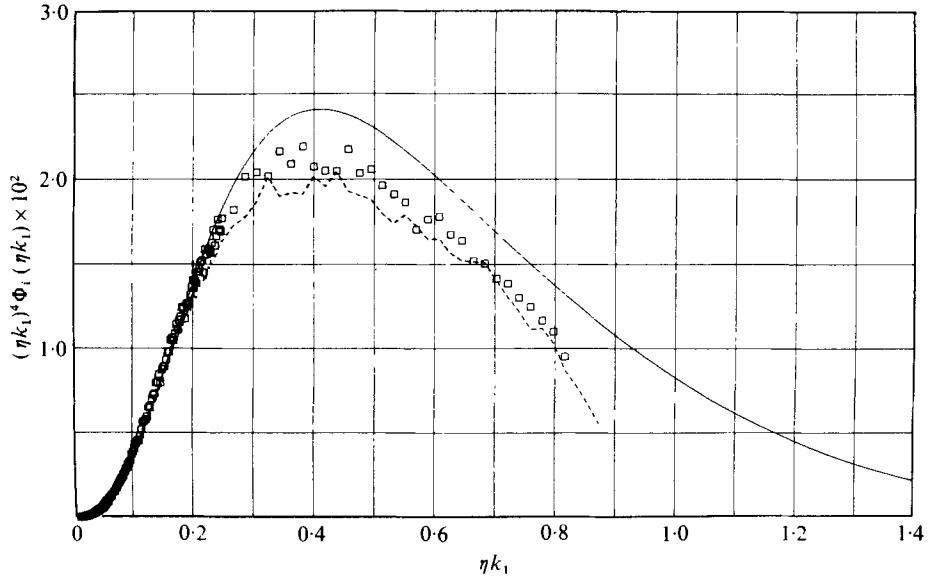

FIGURE 13. Normalized fourth moment of cross-component velocity spectra for two-dimensional wake flow; $R_\lambda = 182$. □, u_2 spectrum; – – –, u_3 spectrum; ——, computed spectrum.

to obtain values of η/l_w that are acceptable from the standpoint of spatial resolution. The measurements for the present experiments were carried out at $x/d = 70$ on the jet centre-line. In order to minimize wire-length attenuation effects and yet achieve a reasonably high R_λ, the jet facility could not be operated at its maximum output. The resulting operating conditions gave $R_\lambda = 626$ and $\eta/l_w = 0{\cdot}44$ (table 1). Figure 15

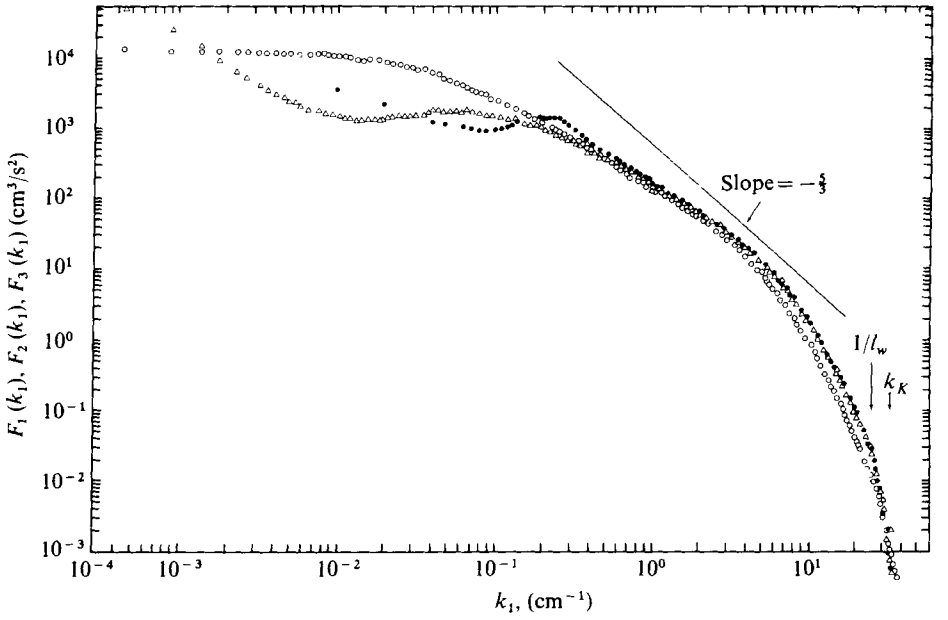

FIGURE 14. One-dimensional energy spectra of the velocity-component fluctuations in the $R_\lambda = 182$ wake flow. ○, u_1 spectrum, $F_1(k_1)$; ●, u_2 spectrum, $F_2(k_1)$; △, u_3 spectrum, $F_3(k_1)$.

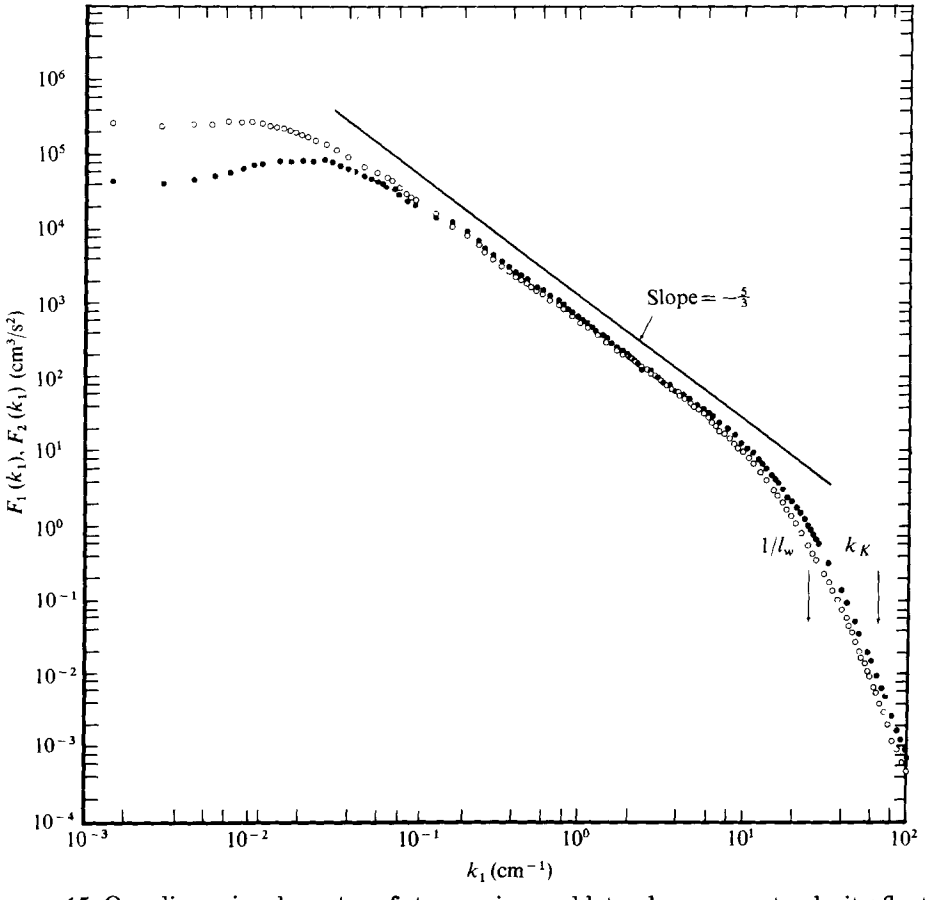

FIGURE 15. One-dimensional spectra of streamwise- and lateral-component velocity fluctuations for an axisymmetric jet; $Re = 3{\cdot}7 \times 10^5$, $x/d = 70$, $r/d = 0$. ○, $F_1(k_1)$; ●, $F_2(k_1)$.

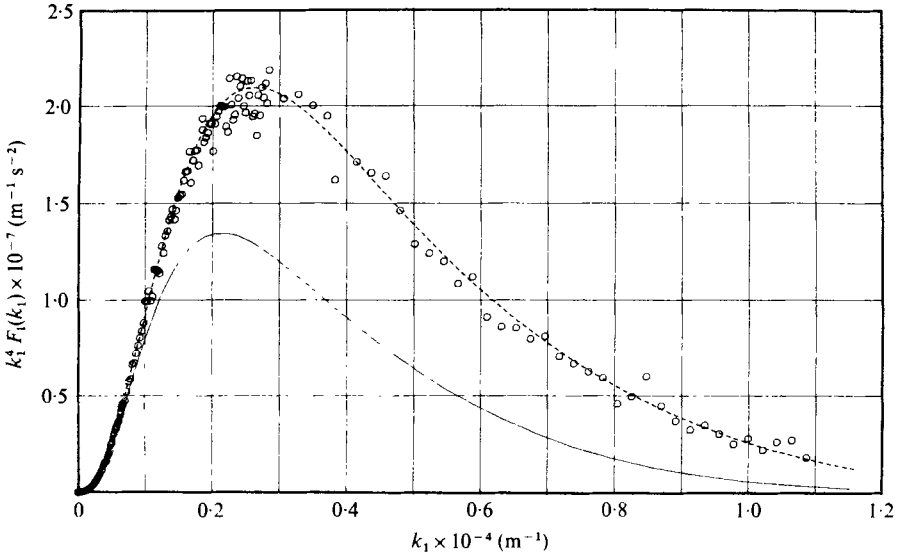

FIGURE 16. Dimensional fourth moment of streamwise spectrum for jet flow. ○, measured spectrum; ---, eleventh-order least-squares curve fit to data; ——, Lumley-corrected spectrum.

shows measurements of the $F_1(k_1)$ and $F_2(k_1)$ spectra in dimensional form. The measured spectra were corrected for noise. Analysis of the data indicates that neither relations (9) nor relations (10) are satisfied and the flow appears to be locally anisotropic. Relations (7) are also not satisfied (table 2) as the ratio $\overline{(\partial u_1/\partial t)^2}/\overline{(\partial u_2/\partial t)^2}$, equivalent to the spatial-derivative ratio from Taylor's approximation, is 0·70, which is far from the isotropic value of 0·50. Unfortunately, the turbulent intensities in a free jet are quite large, e.g. a typical value is $\tilde{u}_1/\overline{U}_1 \approx 0{\cdot}30$ on the centre-line of a self-preserving axisymmetric jet, where the tilde denotes the r.m.s. value. The interpretation of time spectra and directly computed statistics such as moments of derivative signals measured in high intensity turbulent flows is complex, as previously pointed out, because Taylor's approximation is not valid for such flows. A correction for effects caused by deviations from Taylor's hypothesis on interpreting the mean-square velocity derivatives can be obtained from (35) and (39). For the u_2 component, one can show that

$$\overline{\left(\frac{\partial u_2}{\partial t}\right)^2} = \overline{U}_1^2 \overline{\left(\frac{\partial u_2}{\partial x_1}\right)^2} \left[1 + \frac{\overline{u_1^2}+\overline{u_3^2}}{\overline{U}_1^2} + \frac{1}{2}\frac{\overline{u_2^2}}{\overline{U}_1^2}\right]. \tag{55}$$

The resulting ratio $\overline{(\partial u_1/\partial x_1)^2}/\overline{(\partial u_2/\partial x_1)^2}$ computed from (35) and (55) is 0·63, which is somewhat greater than the value 0·58 for the lower R_λ wake.

The importance of correcting for deviations from Taylor's hypothesis in investigating spectral shapes can be realized from considering figures 16–20. Figure 16 shows the effect of the Lumley correction on the dimensional fourth moment of the jet spectrum. The corrected spectrum was computed from (29) using an eleventh-order least-squares polynomial fit to the measured data in the form of (54). The eleventh-order fit and the measured spectral data are also shown. At $k_1 \approx 5800\,\mathrm{m}^{-1}$, which corresponds to Kolmogorov's wavenumber, the measured spectral value is 238%

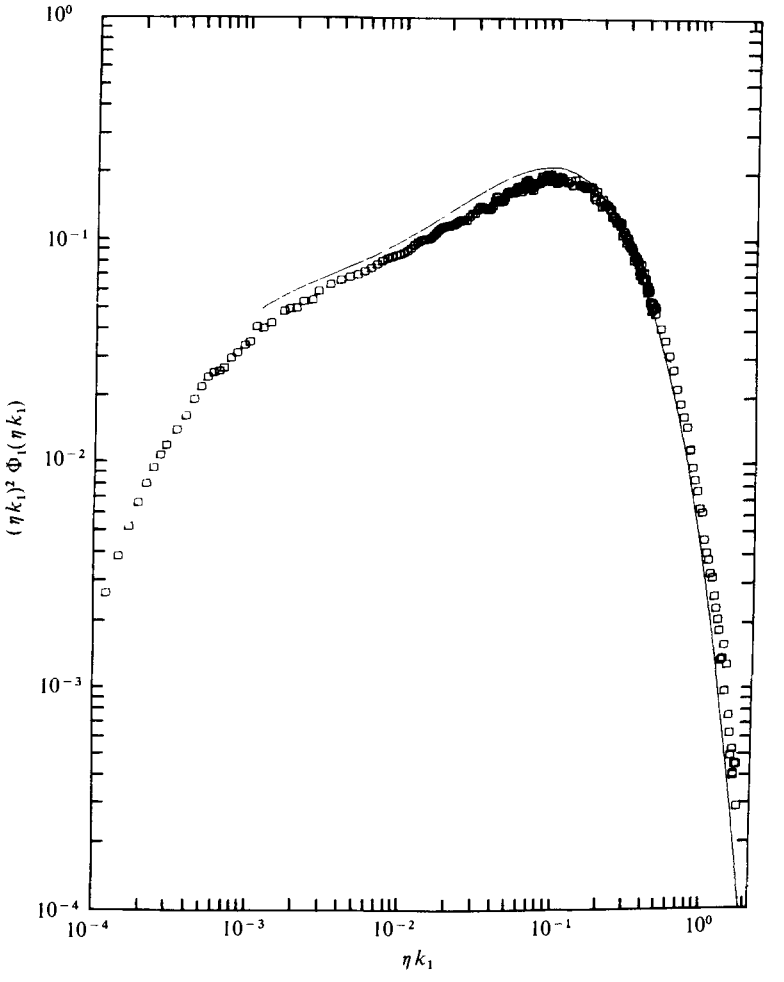

FIGURE 17. Second moment of normalized jet spectra. □, measured spectrum; ——, corrected spectrum.

greater than the corrected spectral value. The various necessary criteria posed by Lumley for applicability of his solution were satisfied for the entire region over which the correction was applied. The effect of the correction on the normalized spectrum is somewhat diminished as the corrected dimensional spectrum is divided by the corrected value of the dissipation rate to the appropriate power. The normalized second moment of the measured spectrum, $(\eta_m k_1)^2 \Phi_1^m(\eta_m k_1)$, and of the corrected spectrum, $(\eta k_1)^2 \Phi_1(\eta k_1)$, are presented in figures 17 and 18. η_m and η refer to the Kolmogorov microscales computed from the measured and corrected dissipation values, respectively. Similarly, normalization of the measured and corrected dimensional spectra was performed using the appropriate dissipation values. Figure 19 shows the normalized fourth moment of the measured and corrected jet spectra, the $R_\lambda = 411$ boundary-layer data of Mestayer (1975), and the low R_λ ($R_\lambda = 138$) cylinder wake data, previously presented in figure 5. The boundary-layer and corrected jet spectra, which have similar values of R_λ, agree quite well. Mestayer's data were obtained in a stratified boundary

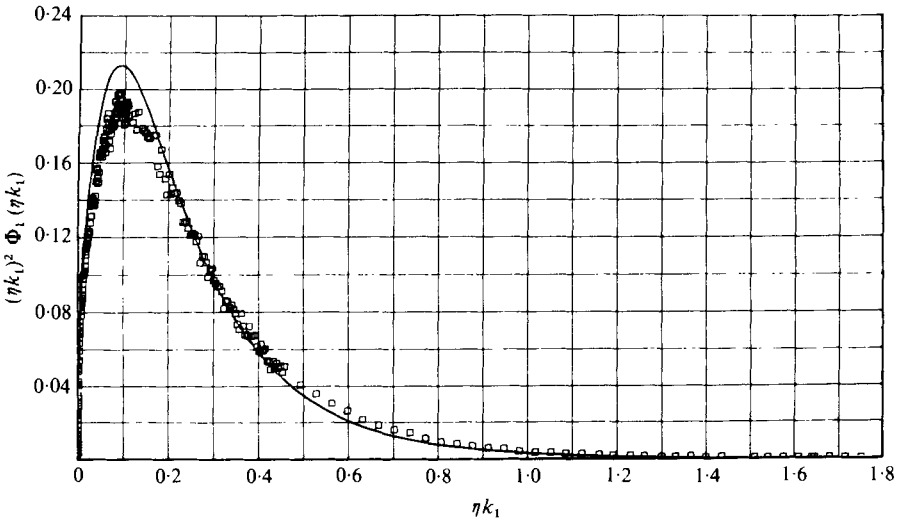

FIGURE 18. Second moment of normalized jet spectra. □, measured spectrum; ——, corrected spectrum.

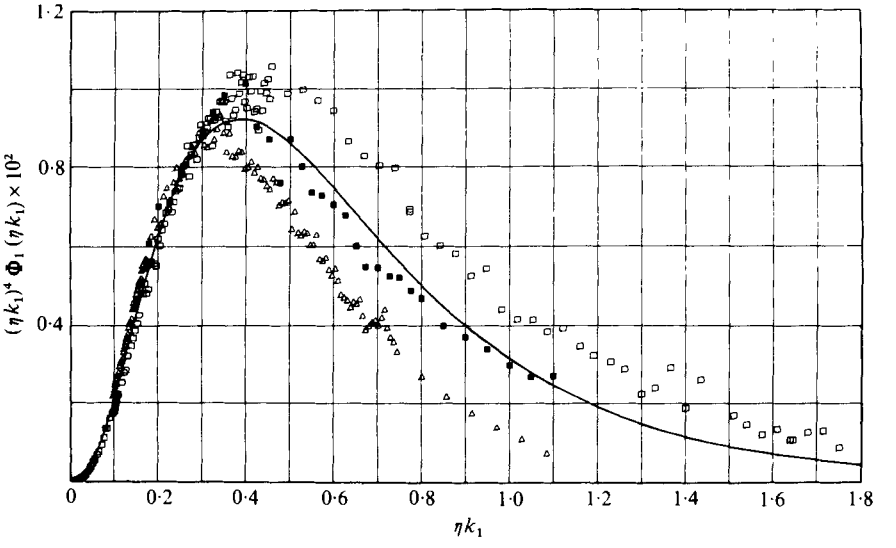

FIGURE 19. Fourth moments of normalized spectra. □, measured jet spectrum; ——, corrected jet spectrum; △, cylinder-wake spectrum, $R_\lambda = 138$; ▲, Mestayer, boundary layer, $R_\lambda = 411$.

layer over water and the turbulent intensities were about 9 %. Lumley's correction was not applied to Mestayer's data in view of the low intensity.

The area under the normalized fourth-moment curves for the jet flow was determined after extrapolating the high wavenumber tails to zero using least-squares polynomial fits as before. If the flow is assumed locally isotropic, (12) gives

$$S^m(\partial u_1/\partial x_1) = -1{\cdot}01$$

and the corrected value $S(\partial u_1/\partial x_1)$ is $-0{\cdot}80$. The value computed directly from the $\partial u_1/\partial t$ signal is $-0{\cdot}67$. From (41), the corrected directly measured value of $S(\partial u_1/\partial x_1)$

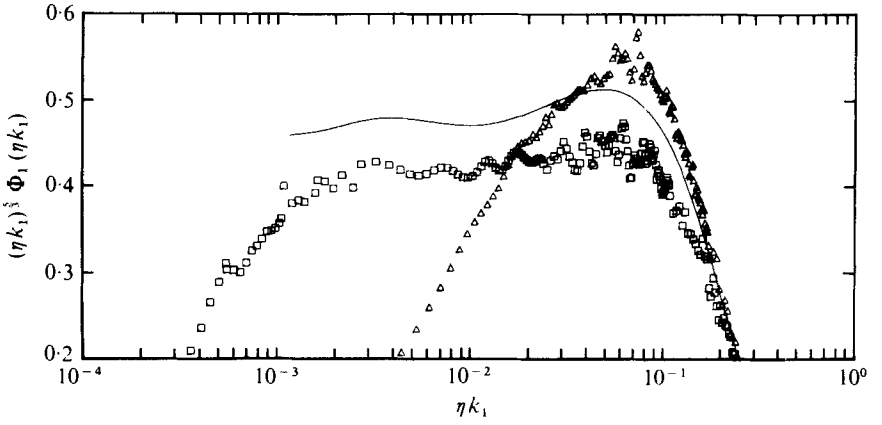

FIGURE 20. Universal constant. □, from measured jet spectrum; ——, from corrected jet spectrum; △, from cylinder-wake spectrum, $R_\lambda = 138$.

is $-0{\cdot}68$, which is 18 % lower in magnitude than the value obtained from (12). Thus (11) appears to be a better approximation in the high R_λ jet flow than in the lower R_λ wake flow discussed previously. The directly measured skewness of the second derivative $\partial^2 u_1/\partial t^2$ was found to be 0·115. No correction for effects caused by deviations from Taylor's approximation was applied or derived, so the significance of the non-zero value with respect to the existence of local isotropy was not determined. The apparent α_1 values are shown in figure 20. The jet results exhibit a saddle-like effect, a minimum occurring in the apparent inertial subrange at a wavenumber of about $\eta k_1 = 10^{-2}$. This minimum is considered to be real and perhaps can be attributed to the double-structure nature of the flow field, i.e. a large-scale vortex-like motion interacting with and driving the fine-scale turbulence. The values α_1^m from the measured spectrum are about $0{\cdot}43 \pm 0{\cdot}02$, which seems quite low, whereas the corrected values are about 0·48. Kholmyanskiy (1972) found a large increase in α_1 when attempting to correct for deviations from Taylor's hypothesis. Using $\overline{U}_1 + u_1$, the instantaneous longitudinal velocity component, as the correct convection velocity, he reported an increase from 0·45 (using $\overline{U}_1$) to 0·62. His measurements were carried out over the Russian Steppes, where the turbulent intensity would presumably be large, although no values of turbulent intensity were given.

The computed Lumley correction for the measured dimensional spectrum $F_1(k_1)$ extends into the lower wavenumber region as far as $k_1 = 7\ \mathrm{m}^{-1}$, where the 'true' or corrected spectral value is 4 % lower than the measured value. Correction of the cross-component spectrum using Lumley's model has yet to be carried out. Thus any definite conclusions regarding the existence of local isotropy from such criteria as (9) or (10) in the high intensity jet flow cannot be formed until all the appropriate corrections are made. Some of the above jet results seem to contradict the findings of Gibson (1963). He found that the relationship between the cross-component spectra and the streamwise spectrum was consistent with local isotropy and also that the three velocity-component intensities were nearly equal on the jet centre-line. The results of the present study were that $\tilde{u}_1/\overline{U}_1 = 0{\cdot}29$ and $\tilde{u}_2/\overline{U}_1 = 0{\cdot}24$, which are nearly identical to the results obtained by Wygnanski & Fiedler (1969). The fact that Gibson's u_1 and u_2 component intensities were nearly equal would correspond to a relative increase in the

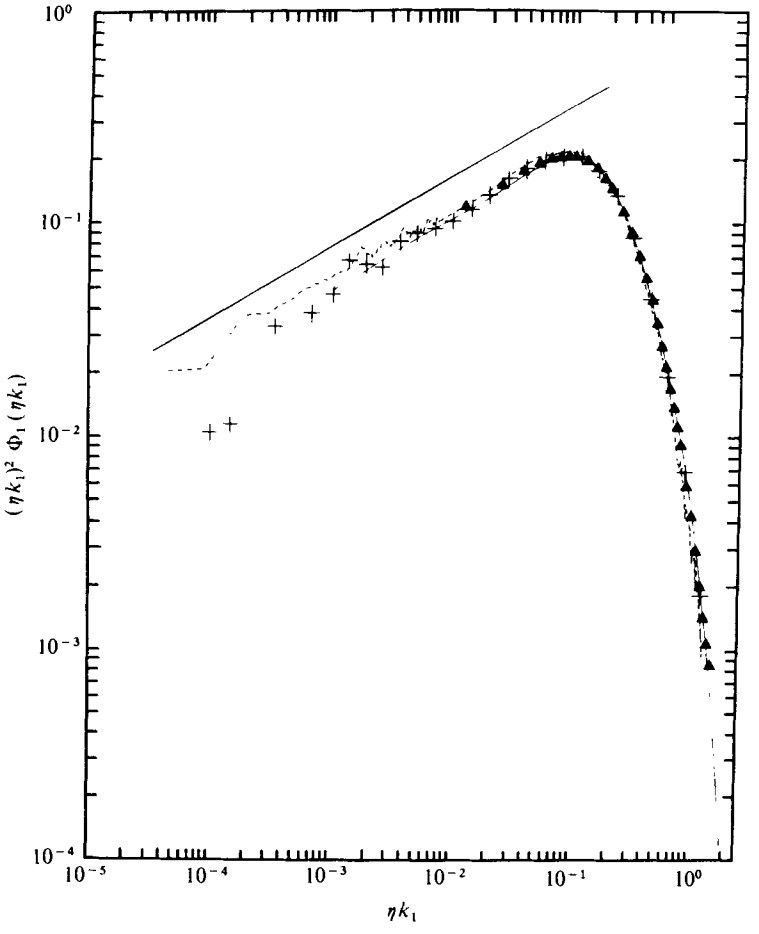

FIGURE 21. Second moments of high Reynolds number normalized spectra. ——, Lumley-corrected GUMBO spectrum; – – –, FS II spectrum; ▲, Wyngaard spectrum; +, Williams spectrum. Solid straight line has a slope of $+\frac{1}{3}$.

u_2 spectral level at least in the lower wavenumbers and perhaps into the apparent inertial subrange. Wire-length attenuation was certainly also a factor in Gibson's data as η/l_w was 0·14 for his study, which according to Wyngaard (1969) would lead to underestimation of ϵ by 25% and significant attenuation for $\eta k_1 > 0{\cdot}1$ (Wyngaard 1968). In view of this and the disagreement in turbulence intensity values with more recent results, Gibson's data were not considered further.

5.3. *High Reynolds number spectra*

Recently, many attempts to obtain high quality data on the fine-scale structure of turbulent velocity fields in high Reynolds number geophysical flows have been undertaken by several groups including our own at UCSD. Of all the geophysical flows, the surface layer of the atmospheric boundary layer proves particularly attractive because standard laboratory instrumentation is more than adequate to provide the required measurements. High Reynolds number spectral data from four experiments on the atmospheric boundary layer are shown in figures 21–25. The GUMBO spectral results

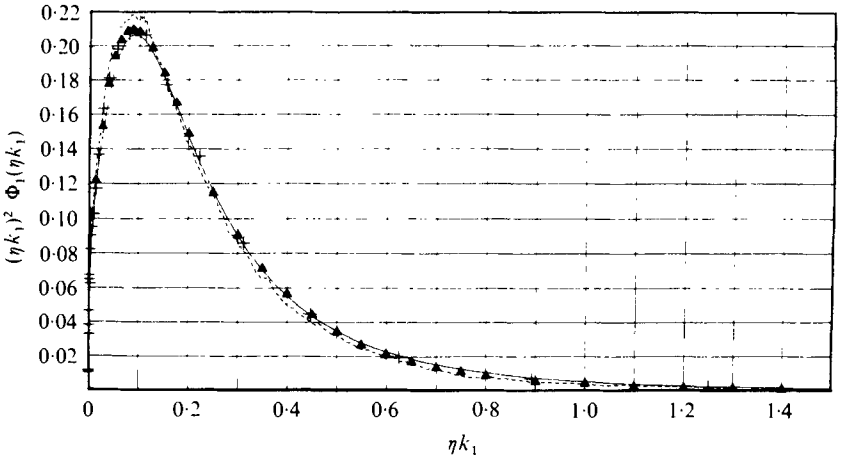

FIGURE 22. Normalized second moments of high Reynolds number spectra. ——, Lumley-corrected GUMBO spectrum; – – –, FS II spectrum; ▲, Wyngaard spectrum; +, Williams spectrum.

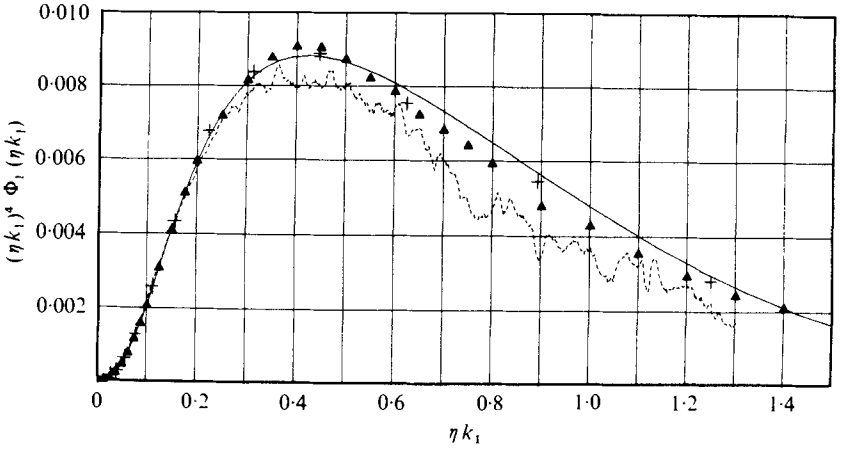

FIGURE 23. Normalized fourth moments of high Reynolds number spectra. ——, Lumley-corrected GUMBO spectrum; – – –, FS II spectrum; ▲, Wyngaard spectrum; +, Williams spectrum.

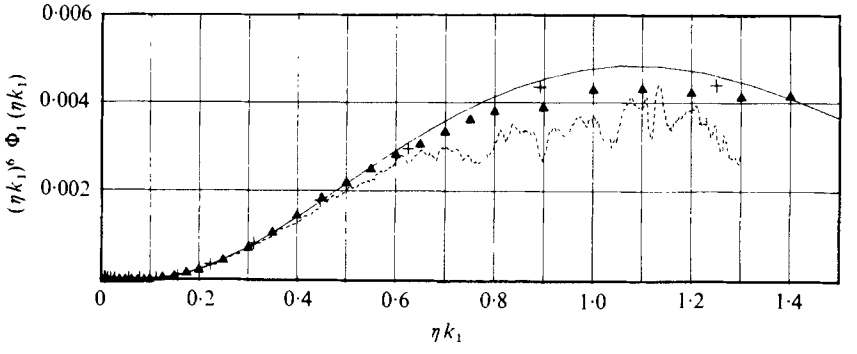

FIGURE 24. Normalized sixth moments of high Reynolds number spectra. ——, Lumley-corrected GUMBO spectrum; – – –, FS II spectrum; ▲, Wyngaard spectrum; +, Williams spectrum.

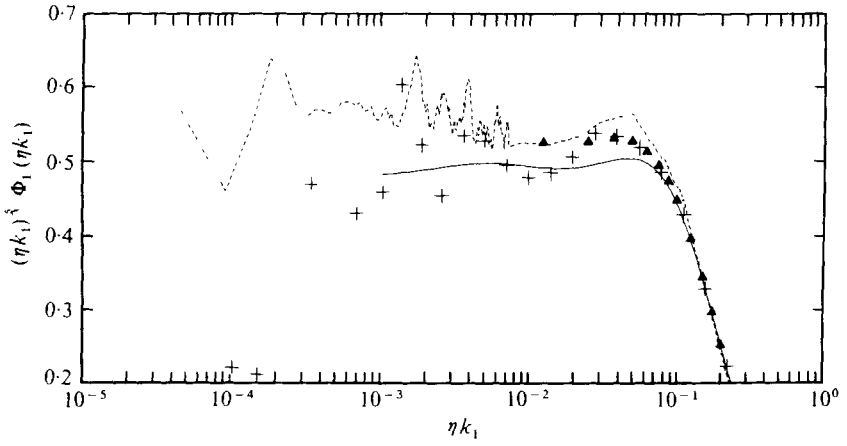

FIGURE 25. Universal constants from high Reynolds number data. ——, Lumley-corrected GUMBO data; – – –, FS II data; ▲, Wyngaard data; +, Williams data.

were obtained over a 15 min period with $R_\lambda = 7000$ (see table 1). The turbulent intensities measured over this time period were $\tilde{u}_1/\overline{U}_1 = 0{\cdot}18$, $\tilde{u}_2/\overline{U}_1 = 0{\cdot}29$ and $\tilde{u}_3/\overline{U}_1 = 0{\cdot}069$, where u_1 and u_2 are the horizontal components and u_3 the vertical component of the turbulent velocity field. Lumley's correction was applied to the measured spectral data and the corrected spectrum was determined from (29) using a ninth-order least-squares polynomial fit to the measured spectrum in the form of (54). η/l_w was 0·68 so the spatial resolution of the hot wire was adequate since, according to Wyngaard's (1968) analysis, the spectral attenuation is about 10 % at $\eta k_1 = 1{\cdot}5$. No noise correction was applied to the data. The FS II data were obtained over two 20 min periods for which the mean wind speed was steady at 11 m/s, $\tilde{u}_1/\overline{U}_1$ was 0·11 and the resulting R_λ was 13 000. These are the highest R_λ data available, although they should be interpreted as a representative lower bound for this case because of the already discussed line noise problem. Lumley's correction was not applied to the spectral data in view of the lower intensity and the uncertainty discussed above. η/l_w was 0·82 so wire-length attenuation is negligible over the wavenumber region of interest.

The Kolmogorov normalized spectra of the derivative $\partial u_1/\partial x_1$ are presented in figure 21. An inertial subrange appears to exist for more than one decade in wavenumber in the Lumley-corrected GUMBO data and for more than two decades in the FS II data as is apparent from the agreement with a $+\frac{1}{3}$ slope, indicated by the solid straight line. Also shown for comparison are the surface-layer data of Wyngaard (see Wyngaard & Pao 1972) and Williams (1974), which show good agreement with the present data for wavenumbers $\eta k_1 > 10^{-3}$. Wyngaard's data represent, for a given normalized wavenumber, the average of eight separate spectral estimates, each determined from a 15 min sample of the velocity derivative. The R_λ values differ for each estimate, varying from 1600 to 5000 with an average value of about 2800. Wyngaard used (36) to correct his measured values of ϵ, but no correction was applied to the measured dimensional spectra. Thus the normalized spectra are only partially corrected for effects caused by deviations from Taylor's approximation. During Wyngaard's experiments, $\tilde{u}_1/\overline{U}_1$ was on average about 16 %. As the spectral data were averaged over several runs with a range of Reynolds numbers, and as the ϵ values were corrected,

further corrections using Lumley's model were not attempted. No noise corrections were applied. Williams' data were noise corrected but no corrections to the measured spectra nor the value of ϵ were made for deviations from Taylor's hypothesis. Only the u_1 component was measured and $\tilde{u}_1/\overline{U}_1$ was reported to be 10 %. Figure 22 shows the normalized derivative spectra on a linear–linear plot. The spectra agree quite well and exhibit peak values of about 0·21 at normalized wavenumbers of about 0·09–0·10. Comparison with figure 4 shows that the peak value decreases with increasing R_λ, while the normalized spectral content in the upper portion of the dissipative region increases with increasing R_λ. The normalized wavenumber at which the peak occurs appears to be invariant with R_λ. Each set of normalized spectral data satisfies the constraint (13) and thus is self-consistent. The fourth moments of the normalized spectra are shown in figure 23. The magnitude and position of the peak values of all four sets of data agree well. The R_λ range is rather large for the data presented in figures 21–25, primarily because of the relatively low value for Williams' data. Williams located his probes quite close to the ground at $z = 2$ m and this is undoubtedly the reason for the relatively small value of λ_g, 2·8 cm, he obtained. The λ_g values from the jet, GUMBO and FS II experiments are 0·76, 11·8 and 20·0 cm respectively. As the turbulent intensity increases with decreasing z the value of $\tilde{u}_1/\overline{U}_1 = 0{\cdot}10$ seems low and possibly this could be attributed to the relatively short averaging time of 234 s. If the measured intensity is indeed low then the true R_λ is larger and also the possibility that the data require correction for deviations from Taylor's hypothesis arises. This would tend to lower the high wavenumber region of the spectrum. In any case the high R_λ normalized spectra appear to collapse together nicely in the high wavenumber region, again indicating the usefulness of Kolmogorov scaling. Values of $S(\partial u_1/\partial x_1)$ inferred from (12) were computed after least-squares polynomial extrapolation to $\eta k_1 = 2{\cdot}0$ for integration. These values are presented in table 3 along with the directly measured value from the $\partial u_1/\partial t$ signal. The ratio of the skewness inferred from (12) to the directly measured value appears to decrease with increasing R_λ, approaching unity at larger R_λ values. That is, the turbulent vorticity budget (11) appears to be a good approximation in the higher R_λ flow fields. The value of this ratio for FS II is undoubtedly less than unity because of the line noise problems mentioned previously, which could cause an overestimation of the directly measured skewness and an underestimation of the skewness value inferred from (12) because of the noise correction procedure.

The sixth moments of the normalized spectra are presented in figure 24 and give some indication of the quality of the fourth-moment data. The peak amplitude appears to occur at a normalized wavenumber of about 1·1. Because of problems with the signal-to-noise ratio and wire-length attenuation, it is not yet possible to determine the entire sixth moment of the normalized spectrum in a high Reynolds number flow.

Values of the 'universal constant' α_1 are presented in figure 25. The corrected GUMBO value is $0{\cdot}50 \pm 0{\cdot}02$ while the FS II value is about $0{\cdot}56 \pm 0{\cdot}03$. These results agree well with those of Williams, who gives a value of $0{\cdot}50 \pm 0{\cdot}03$, and those of Wyngaard & Pao, who obtained $0{\cdot}53 \pm 0{\cdot}02$. The latter found that their α_1 estimates exhibited no stability dependence. No observable trend in the value of α_1 with increasing R_λ was apparent.

For the GUMBO experiment, the shear-stress co-spectrum was measured directly (Champagne *et al.* 1977). The plot of frequency times the co-spectrum peaks at about a

Flow	R_λ	(a) $-S\left(\frac{\partial u_1}{\partial x_1}\right)$	(b) $116\int_0^\infty y^4\Phi_1^m(y)\,dy$	(b) $116\int_0^\infty x^4\Phi_1(x)\,dx$	(b)/(a)	$\frac{-S}{K^{\frac{3}{2}}}$
Cylinder wake flow	182	0·48	0·64	0·64	1·33	0·25
Axisymmetric jet	626	0·68	1·01	0·80	1·18	0·25
Atmospheric boundary layer, Wyngaard	2800	0·74–0·81	—	0·96†	1·37–1·13	—
Atmospheric boundary layer, GUMBO	7000	0·74–0·81	1·10	0·95	1·28–1·19	0·22–0·24
Atmospheric boundary layer, FS II	13000	0·89	0·82	0·82	0·92	0·25

$y = \eta_m k_1, \quad x = \eta k_1.$

† Partially corrected as explained in text.

TABLE 3

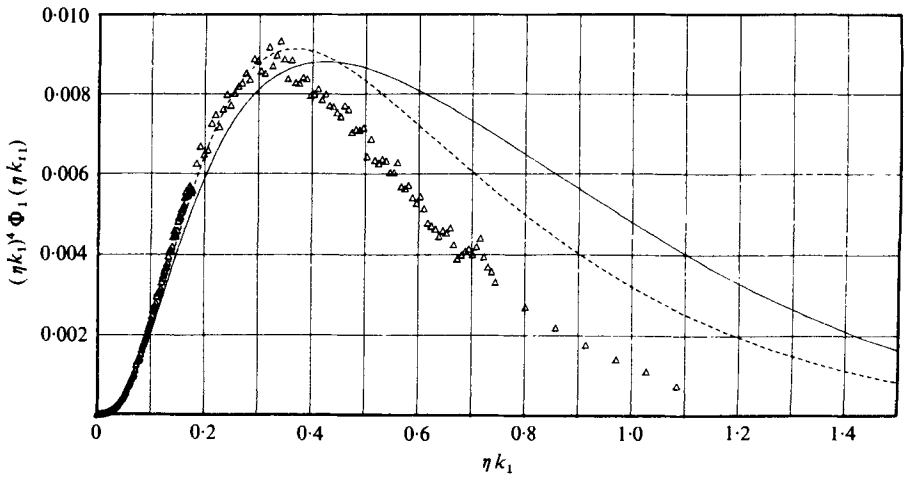

FIGURE 26. Evolution of fourth moment of normalized spectra with turbulence Reynolds number. △, cylinder-wake spectrum, $R_\lambda = 138$; – – –, Lumley-corrected jet spectrum, $R_\lambda = 626$; ——, Lumley-corrected GUMBO spectrum, $R_\lambda = 7000$.

normalized frequency $fz/\overline{U}_1$ of 0·05, which agrees well with the results of Kaimal *et al.* (1972) for similar stability conditions. Thus a measure of the wavenumber region characterized by shear production of turbulent energy is $k_p \approx 0{\cdot}077\ \mathrm{m}^{-1}$. As $k_K = 1538\ \mathrm{m}^{-1}$, then $k_K/k_p \approx 2 \times 10^4$, which seems large enough to expect inertial and dissipative local isotropy. Further, sonic anemometer results with a spatial resolution of 20 cm indicate that the ratio of $\frac{4}{3}$ between $F_3(k_1)$ and $F_1(k_1)$ is realized at a wavenumber of $2m^{-1}$, or $\eta k_1 \approx 1 \times 10^{-3}$. Although no fine-scale measurements of u_2 and u_3 fluctuations are available for GUMBO or the other atmospheric flows presented here, it will be assumed that the fine-scale structure of these flow fields is isotropic on the basis of the GUMBO results and those of Kaimal *et al.* (1972).

The Reynolds number dependence of the high wavenumber regions of the normalized spectra is summarized in figure 26. The $R_\lambda = 138$ wake data, the corrected jet data and the corrected GUMBO atmospheric-boundary-layer data are presented. As R_λ increases the normalized spectrum function $\Phi_1(\eta k_1)$ decreases in the lower part of the dissipative wavenumber region up to $\eta k_1 \approx 0{\cdot}35$ and increases at the higher end, i.e. for $\eta k_1 > 0{\cdot}45$. The maximum in the normalized fourth moment of Φ_1 decreases slightly in magnitude and moves towards larger wavenumbers as R_λ increases. In the framework of the modified hypothesis this is the expected behaviour of Φ_1 from consideration of the constraints (12) and (13), and the observed increase in $-S(\partial u_1/\partial x_1)$ with increasing R_λ (Wyngaard & Pao 1972). Wyngaard & Tennekes (1970) pointed out that systematic departures from scaling laws which use a mean or average dissipation rate should be expected. The departures, attributed to the spatial variation of dissipation, would depend on the Reynolds number. Table 3 presents values of the ratio

$$-S\left(\frac{\partial u_1}{\partial x_1}\right) \Big/ K\left[\left(\frac{\partial u_1}{\partial x_1}\right)^2\right]^{\frac{3}{8}},$$

which is remarkably constant over the entire range of Reynolds numbers considered here, again consistent with the modified hypothesis. However, the predicted power-law behaviours $S(\partial u_1/\partial x_1) \sim R_\lambda^{\frac{3}{16}}$ and $K(\partial u_1/\partial x_1) \sim R_\lambda^{\frac{1}{2}}$ tend to overestimate the actual

Flow	$R_\lambda = 138$ (wake flow)	$R_\lambda = 626$ (jet flow)	$R_\lambda = 7000$ (atmospheric-boundary-layer flow)
B_1	$-6{\cdot}7188063E\ 00$	$-1{\cdot}9294144E\ 01$	$-5{\cdot}3474115E\ 00$
B_2	$-8{\cdot}5951979E\ 00$	$-6{\cdot}3374476E\ 00$	$-5{\cdot}7015913E\ 00$
B_3	$-4{\cdot}4856806E\ 00$	$-1{\cdot}8805391E\ 00$	$-1{\cdot}7340985E\ 00$
B_4	$-3{\cdot}0569138E\ 00$	$-1{\cdot}1604677E\ 00$	$-1{\cdot}1595819E\ 00$
B_5	$-1{\cdot}7175563E\ 00$	$-8{\cdot}2677730E-01$	$-7{\cdot}4607554E-01$
B_6	$-6{\cdot}0644193E-01$	$-2{\cdot}9785443E-01$	$-2{\cdot}7277963E-01$
B_7	$-1{\cdot}2747098E-01$	$-2{\cdot}8002934E-02$	$-5{\cdot}5821590E-02$
B_8	$-1{\cdot}5485045E-02$	$1{\cdot}4472714E-02$	$-6{\cdot}4303002E-03$
B_9	$-9{\cdot}9908290E-04$	$5{\cdot}6844623E-03$	$-3{\cdot}8967483E-04$
B_{10}	$-2{\cdot}6312047E-05$	$9{\cdot}0049066E-04$	$-9{\cdot}6258711E-06$
B_{11}		$6{\cdot}9919375E-05$	
B_{12}		$2{\cdot}1865197E-06$	

TABLE 4

variation with R_λ, especially at larger R_λ. Further, examination of figures 23 and 26 indicates that the rate of variation of spectrum shape with R_λ decreases at the larger Reynolds numbers. This brings another consideration to mind. Perhaps Kolmogorov's ideas should not be expected to apply until R_λ is sufficiently large that the vorticity budget (11) is satisfied, i.e. until the turbulent vorticity field is largely decoupled from the (usually anisotropic) structure of the mean flow field. In any case, the available evidence indicates that Kolmogorov scaling leads to normalized spectral functions that are universal in the sense that they apply to the fine-scale dissipative structure of all turbulent flow fields with the same turbulence Reynolds number. The normalized spectral functions vary with turbulence Reynolds number in a manner consistent with the modified hypothesis. The values of the Kolmogorov normalized functions shown in figure 26 can be determined from a least-squares polynomial fit of the form

$$\ln \Phi_1(\eta k_1) = B_1 + B_2 Z + B_3 Z^2 + \ldots + B_{n+1} Z^n, \tag{56}$$

where $Z = \ln(\eta k_1)$ and the coefficients for the three curves shown can be obtained from table 4.

6. Summary and conclusions

The fine-scale structure of many turbulent velocity fields is examined for evidence of universal behaviour and local isotropy. Existing data as well as new results from recent studies of many different flow fields including wakes, jets and the atmospheric boundary layer are investigated. Data interpretation problems are considered, including the effects of concomitant temperature fluctuations on the measured hot-wire signal. Also revealed is the importance of considering the effects on spectra caused by deviations from Taylor's approximation in high intensity flows. Lumley's (1965) model is used to correct the high frequency portion of the measured spectra for those effects. An analytical solution to Lumley's correction equation is presented and applied to the jet and atmospheric-boundary-layer data. Corrections to the jet spectrum indicate that the measured spectrum is overestimated by 200% for frequencies of the order of that corresponding to the Kolmogorov length scale.

The low R_λ flows considered appeared to exhibit dissipative local isotropy, including the cylinder wake flow and the nearly homogeneous shear flow. How well some of the various criteria for the existence of local isotropy were satisfied for these flows is presented and discussed. It is not possible to assess whether the relatively high R_λ axisymmetric jet flow is locally isotropic until all the statistics used in the criteria are corrected for deviations from Taylor's approximation. Kolmogorov scaling of the spectra is shown to lead to normalized spectral functions that are universal in the sense that they describe the fine-scale spectral behaviour of all turbulent flow fields with a similar value of the turbulence Reynolds number. The normalized spectral functions vary with turbulence Reynolds number in a manner consistent with the modified hypothesis of Kolmogorov. Expressions for the Kolmogorov normalized spectral functions at three turbulence Reynolds numbers are given in a polynomial form obtained from least-squares fits to the data. The ratio

$$S\left(\frac{\partial u_1}{\partial x_1}\right) \Big/ \left[K\left(\frac{\partial u_1}{\partial x_1}\right)\right]^{\frac{3}{2}},$$

predicted by Wyngaard & Tennekes (1970) to be independent of R_λ within the framework of the modified hypothesis, is found to be remarkably constant and equal to $-0{\cdot}25$ over the R_λ range 180–13 000 considered here. However, examination of the normalized fourth moments of spectra for various Reynolds numbers indicates that the rate of variation of spectral shape with R_λ decreases at the larger Reynolds numbers. This leads to the speculation that Kolmogorov's ideas do not apply until the turbulence Reynolds number is sufficiently large that the vorticity variance equation reduces to a balance between production by turbulent vortex stretching and viscous dissipation of vorticity. Thus the vorticity budget would be largely independent of the structure of the mean flow field. Further definitive experiments in high R_λ flows are required to investigate the trends shown here and to provide new information relevant to the existence of local isotropy in the fine-scale structure of the velocity field. This is especially true in view of recent results indicating apparent anisotropy of the fine-scale temperature fields for many of the flow fields considered here.

I should like to thank Carl A. Friehe and John C. LaRue for their help and co-operation in carrying out the field experiments and subsequent data reduction. I should also like to thank I. Wygnanski for his co-operation in carrying out the laboratory wake and jet experiments and for his help in the initial phases of the analytical work. Thanks are also due to John C. Wyngaard for his valuable suggestions and comments throughout the course of the study. Acknowledgement is also due to Carl H. Gibson for his continual support and encouragement. I should also like to thank T. K. Deaton for his efforts in designing and constructing the special electronic circuits that made the field experiments successful. I am also grateful to Beth Di Julio and Bobbye Johnson for patiently and expertly typing the manuscript. This work was supported under AFOSR Grants 72-2287 and 77-3172 and NSF Grant ATM 76-23856.

Appendix

The isotropic tensor form for $\overline{\frac{\partial^2 u_1}{\partial x_k \partial x_m}\frac{\partial^2 u_1}{\partial x_l \partial x_n}}$ was required in the reduction of (40). The necessary form of the sixth-order isotropic tensor was determined using the invariance theory as presented by Robertson (1940) with the result

$$\begin{aligned}\overline{\frac{\partial^2 u_i}{\partial x_k \partial x_m}\frac{\partial^2 u_j}{\partial x_l \partial x_n}} = [&\delta_{ij}\delta_{kn}\delta_{lm} + \delta_{ij}\delta_{ln}\delta_{km} + \delta_{ij}\delta_{kl}\delta_{mn} \\ &- \tfrac{1}{6}(\delta_{il}\delta_{jn}\delta_{km} + \delta_{il}\delta_{kn}\delta_{jm} + \delta_{jl}\delta_{in}\delta_{km} + \delta_{jl}\delta_{kn}\delta_{im} \\ &+ \delta_{kl}\delta_{in}\delta_{jm} + \delta_{kl}\delta_{jn}\delta_{im} + \delta_{ik}\delta_{jl}\delta_{mn} + \delta_{jk}\delta_{il}\delta_{mn} \\ &+ \delta_{ik}\delta_{jn}\delta_{lm} + \delta_{ik}\delta_{ln}\delta_{jm} + \delta_{jk}\delta_{in}\delta_{lm} + \delta_{jk}\delta_{ln}\delta_{im})]\overline{\left(\frac{\partial^2 u_1}{\partial x_1^2}\right)^2}. \quad \text{(A 1)}\end{aligned}$$

This expression also proves to be useful in evaluating the viscous dissipation term in the turbulent vorticity budget if one assumes that the fine-scale structure of the turbulent field is locally isotropic. The result is readily shown to be

$$\nu\overline{\frac{\partial \omega_i}{\partial x_j}\frac{\partial \omega_i}{\partial x_j}} = 35\overline{\left(\frac{\partial^2 u_1}{\partial x_1^2}\right)^2} = 35\int_0^\infty k_1^4 F_1(k_1)\,dk_1, \quad \text{(A 2), (A 3)}$$

where (33) has been used.

The production term $\overline{\omega_i \omega_j \partial u_i/\partial x_j}$ in the vorticity budget represents the generation of mean-square vorticity by the interaction of the turbulent straining and turbulent vorticity fields. This term can be evaluated for a locally isotropic velocity field using the isotropic tensor form

$$\begin{aligned}\overline{\frac{\partial u_i}{\partial x_j}\frac{\partial u_k}{\partial x_l}\frac{\partial u_m}{\partial x_n}} = [&\delta_{ij}\delta_{kl}\delta_{mn} - \tfrac{4}{3}(\delta_{ij}\delta_{km}\delta_{ln} + \delta_{ik}\delta_{lj}\delta_{mn} \\ &+ \delta_{im}\delta_{jn}\delta_{kl}) - \tfrac{1}{6}(\delta_{ij}\delta_{kn}\delta_{lm} + \delta_{il}\delta_{kj}\delta_{mn} + \delta_{in}\delta_{kl}\delta_{jm}) \\ &- \tfrac{3}{4}(\delta_{il}\delta_{kn}\delta_{jm} + \delta_{in}\delta_{kj}\delta_{lm}) + \delta_{il}\delta_{km}\delta_{jn} + \delta_{in}\delta_{km}\delta_{lj} \\ &+ \delta_{ik}\delta_{lm}\delta_{jn} + \delta_{ik}\delta_{ln}\delta_{jm} + \delta_{im}\delta_{jl}\delta_{kn} + \delta_{im}\delta_{jk}\delta_{ln}]\overline{\left(\frac{\partial u_1}{\partial x_1}\right)^3}, \quad \text{(A 4)}\end{aligned}$$

which was worked out and kindly furnished by J. Wyngaard. The required production term can therefore be expressed as

$$\overline{\omega_i \omega_j \frac{\partial u_i}{\partial x_j}} = -\frac{35}{2}\overline{\left(\frac{\partial u_1}{\partial x_1}\right)^3}. \quad \text{(A 5)}$$

This allows evaluation from the directly measured $S(\partial u_1/\partial x_1)$ values. Both (A 3) and (A 5) were used to express (11) in its isotropic form given by (12).

REFERENCES

Batchelor, G. K. 1967 *An Introduction to Fluid Dynamics*. Cambridge University Press.

Boston, N. E. J. & Burling, R. W. 1972 *J. Fluid Mech.* **55**, 473.

Bradshaw, P. 1966 *Nat. Phys. Lab. Aero. Rep.* no. 1124.

Bradshaw, P. 1967 *Nat. Phys. Lab. Aero. Rep.* no. 1220.

BUSCH, N. E. 1973 *Boundary-Layer Met.* **4**, 213.

CHAMPAGNE, F. H., FRIEHE, C. A., LARUE, J. C. & WYNGAARD, J. 1977 *J. Atmos. Sci.* **34**, 515.

CHAMPAGNE, F. H., HARRIS, V. G. & CORRSIN, S. 1970 *J. Fluid Mech.* **41**, 81.

CHAMPAGNE, F. H., SLEICHER, C. A. & WEHRMANN, O. H. 1967 *J. Fluid Mech.* **28**, 153.

CHAMPAGNE, F. H., WYGNANSKI, I. & PAO, Y. H. 1976 *J. Fluid Mech.* **74**, 209.

COMTE-BELLOT, G. 1965 *Publ. Sci. Tech. Min. Air (France) Notes Tech.* no. 419.

COMTE-BELLOT, G. & CORRSIN, S. 1971 *J. Fluid Mech.* **48**, 273.

CORRSIN, S. 1957 *Proc. 1st Naval Hydro. Symp., Nat. Acad. Sci. Math. Res. Counc.* publ. 515, p. 373.

CORRSIN, S. 1959 *J. Geophys. Res.* **64**, 2134.

ELDERKIN, C. E. 1966 Ph.D. thesis, Dept. of Atmospheric Sciences, University of Washington, Seattle.

FAVRE, A. J. 1965 *J. Appl. Mech.* **87**, 241.

FISHER, M. J. & DAVIES, P. O. A. L. 1964 *J. Fluid Mech.* **18**, 97.

GIBSON, C. H. & MASIELLO, P. 1972 *Proc. Symp. Statistical Models and Turbulence. Lecture Notes in Physics*, vol. 12. Springer.

GIBSON, C. H. & SCHWARZ, W. H. 1963. *J. Fluid Mech.* **16**, 365.

GIBSON, C. H., STEGEN, G. R. & WILLIAMS, R. B. 1970 *J. Fluid Mech.* **41**, 153.

GIBSON, M. M. 1963 *J. Fluid Mech.* **15**, 161.

GRANT, H. L., STEWART, R. W. & MOILLIET, A. 1962 *J. Fluid Mech.* **12**, 241.

GURVICH, A. S. & YAGLOM, A. M. 1967 *Phys. Fluids Suppl.* **10**, S 59.

HESKESTAD, G. 1965 *J. Appl. Mech.* **87**, 735.

KAIMAL, J. C., WYNGAARD, J. C., ISUMI, Y. & COTÉ, O. R. 1972 *Quart. J. Roy. Met. Soc.* **98**, 563.

KÁRMÁN, TH. VON & HOWARTH, L. 1938 *Proc. Roy. Soc.* A **164**, 192.

KHOLMYANSKIY, M. Z. 1972 *Izv. Atmos. Ocean. Phys.* **8**, 472.

KISTLER, A. L. & VREBALOVICH, T. 1966 *J. Fluid Mech.* **26**, 37.

KOLMOGOROV, A. N. 1941 *Dokl. Akad. Nauk SSSR* **30**, 301.

KOLMOGOROV, A. N. 1962 *J. Fluid Mech.* **13**, 82.

KUO, A. 1970 Ph.D. thesis, Dept. of Mechanics, Johns Hopkins University.

KUO, A. & CORRSIN, S. 1972 *J. Fluid Mech.* **56**, 447.

LAUFER, J. 1954 *N.A.C.A. Rep.* no. 1174.

LUMLEY, J. L. 1964 *J. Atmos. Sci.* **21**, 99.

LUMLEY, J. L. 1965 *Phys. Fluids* **8**, 1056.

MESTAYER, P. G. 1975 Thèse de Docteur-Ingénieur, Institut de Mécanique Statistique de la Turbulence, Université de Marseille, France.

OBOUKHOV, A. M. 1962 *J. Fluid Mech.* **13**, 77.

PANCHEV, S. 1971 *Random Functions and Turbulence.* Pergamon.

PAO, Y. H. 1965 *Phys. Fluids* **8**, 1063.

PAO, Y. H., HANSEN, S. D. & MACGREGOR, G. R. 1969 *Boeing Sci. Res. Lab. Doc.* D1-82-0863.

POND, S., SMITH, S. D., HAMBLIN, P. F. & BURLING, R. W. 1966 *J. Atmos. Sci.* **23**, 376.

POND, S., STEWART, R. W. & BURLING, R. W. 1963 *J. Atmos. Sci.* **20**, 319.

ROBERTSON, H. P. 1940 *Proc. Camb. Phil. Soc.* **36**, 209.

ROSHKO, A. 1960 *J. Fluid Mech.* **10**, 348.

SHEIH, C. M., TENNEKES, H. & LUMLEY, J. L. 1971 *Phys. Fluids* **14**, 201.

STEGEN, G. R., GIBSON, C. H. & FRIEHE, C. A. 1973 *J. Phys. Ocean.* **3**, 86.

STEWART, R. W. & TOWNSEND, A. A. 1951 *Phil. Trans. Roy. Soc.* A **243**, 359.

STEWART, R. W., WILSON, J. R. & BURLING, R. W. 1970 *J. Fluid Mech.* **41**, 141.

TAYLOR, G. I. 1938 *Proc. Roy. Soc.* A **164**, 476.

TAYLOR, R. J. 1955 *Austr. J. Phys.* **8**, 535.

TENNEKES, H. & LUMLEY, J. L. 1972 *A First Course in Turbulence.* MIT Press.

TENNEKES, H. & WYNGAARD, J. C. 1972 *J. Fluid Mech.* **55**, 93.

UBEROI, M. S. & FREYMUTH, P. 1969 *Phys. Fluids* **12**, 1359.
WEILER, H. S. & BURLING, R. W. 1967 *J. Atmos. Sci.* **24**, 653.
WILLIAMS, R. M. 1974 Ph.D. thesis, Oregon State University, Corvallis.
WILLS, J. A. B. 1964 *J. Fluid Mech.* **20**, 417.
WYGNANSKI, I. & FIEDLER, H. 1969 *J. Fluid Mech.* **38**, 577.
WYNGAARD, J. C. 1968 *J. Sci. Instrum.* **1**, 1105.
WYNGAARD, J. C. 1969 *J. Sci. Instrum.* **2**, 983.
WYNGAARD, J. C. 1971 *J. Fluid Mech.* **48**, 763.
WYNGAARD, J. C. & PAO, Y. H. 1972 *Proc. Symp. Statistical Models and Turbulence. Lecture Notes in Physics*, vol. 12. Springer.
WYNGAARD, J. C. & TENNEKES, H. 1970 *Phys. Fluids* **13**, 1962.
YAGLOM, A. M. 1966 *Dokl. Akad. Nauk SSSR* **166**, 49.